10/11/12/96 SD1

SANDIA REPORT

SAND96-8247 • UC–1409
Unlimited Release
Printed July 1996

Eigenvalue Analysis and Calculations for the Deflagration of Porous Energetic Materials in the Merged-Flame Regime

Nenad Ilincic and Stephen B. Margolis

Prepared by
Sandia National Laboratories
Albuquerque, New Mexico 87185 and Livermore, California 94551
for the United States Department of Energy
under Contract DE-AC04-94AL85000

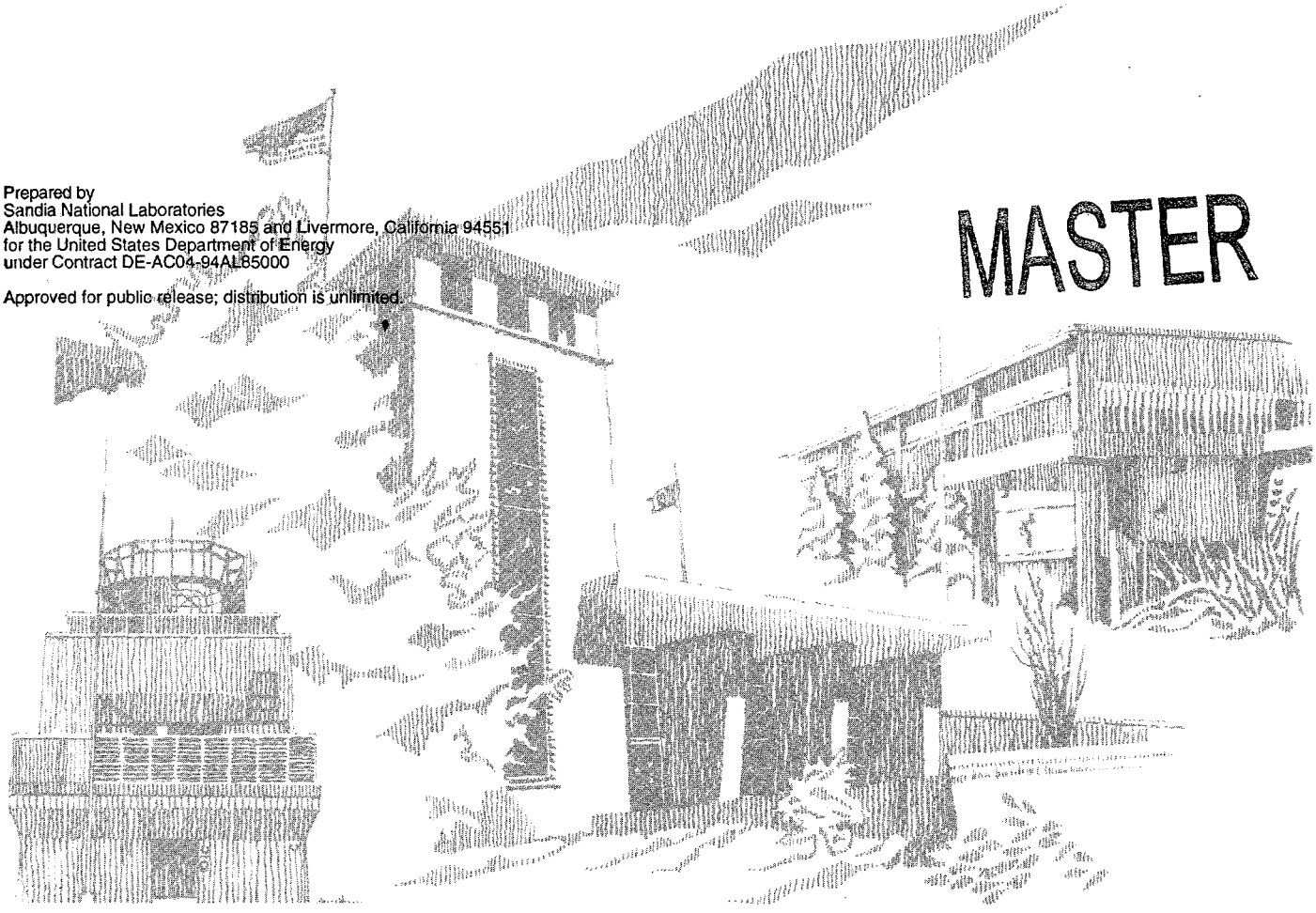

SAND96-8247
Unlimited Release
Printed July 1996

EIGENVALUE ANALYSIS AND CALCULATIONS FOR THE DEFLAGRATION OF POROUS ENERGETIC MATERIALS IN THE MERGED-FLAME REGIME *

NENAD ILINCIC† and STEPHEN B. MARGOLIS‡

†Center for Energy and Combustion Research
Department of Applied Mechanics and Engineering Sciences
University of California, San Diego
La Jolla, California 92093-0411 USA

‡Combustion Research Facility, Mail Stop 9052
Sandia National Laboratories
Livermore, California 94551-0969 USA

Abstract

Analytical and numerical calculations of the structure and burning rate of a deflagrating porous energetic material are presented for the limiting case of merged condensed and gas-phase reaction zones. The reaction scheme is modeled by a global two-step mechanism, applicable to certain types of degraded nitramine propellants and consisting of sequential condensed and gaseous steps. Taking into account important effects due to multiphase flow and exploiting the limit of large activation energies, a theoretical analysis may be developed based on activation-energy asymptotics. For steady, planar deflagration, this leads to an eigenvalue problem for the inner reaction-zone, the solution of which determines the burning rate. Numerical solutions give a reasonably complete description of the dependence of the structure and burning rate on the various parameters in the problem, and show excellent agreement with analytical results that are obtained in a more limited parameter regime in which most of the heat release is produced by the condensed-phase reaction and the porosity of the solid is small. These calculations indicate the significant influences of two-phase flow and the multiphase, multi-step chemistry on the deflagration structure and the burning rate, and thus serve to define an important parameter regime that supports the intrusion of the primary gas flame into the two-phase condensed decomposition region at the propellant surface.

*Work supported by the U. S. Department of Energy under Contract DE-AC04-94AL85000.

EIGENVALUE ANALYSIS AND CALCULATIONS FOR THE DEFLAGRATION OF POROUS ENERGETIC MATERIALS IN THE MERGED-FLAME REGIME

1. Introduction

There is a rapidly growing interest within the fields of propulsion and pyrotechnics in the combustion behavior of porous energetic materials. In these types of problems, the porous nature of the material arises from a certain degree of metastability which, after either a prolonged existence and/or exposure to an abnormal thermal environment, leaves the material in a degraded state that is characterized by changes in chemical composition and a significantly higher porosity relative to the original pristine propellant. As a result, the gas-phase species occupying the voids consist of various products of decomposition, and various two-phase-flow effects associated with different velocities and properties of the condensed and gaseous species have a significant effect on the structure and propagation velocity of the combustion wave.

Although a number of relatively complete formulations have been proposed for analyzing combustion phenomena involving multiphase flow,[1] they generally involve one or more constitutive relations that are required to close the model, and are difficult to analyze, both because of the wide range of physical phenomena associated with such systems and the highly nonlinear nature of any two-phase-flow combustion problem. Accordingly, early two-phase work in this area tended to alleviate some of the difficulties by treating the two-phase medium as a single phase with suitably "averaged" properties.[2,3] Unfortunately, such models effectively require the velocity (and temperature) of each phase to be identical, precluding any analysis of two-phase flow effects on the combustion process. More recently, however, it has proven possible to analyze deflagration models for porous energetic materials that explicitly involve multiphase flow.[4-11] These studies have largely been applicable to nitramine propellants, such as HMX and, in some cases, RDX, that are characterized by a liquid melt region in which extensive bubbling in an exothermic foam layer occurs. In some cases,[4-6] two-phase flow effects were confined to this layer, while in the more recent of these studies,[7-11] the solid material was assumed to be sufficiently porous such that two-phase flow effects were significant throughout the multiphase preheat region. In order to focus clearly on the effects of two-phase flow in these problems, chemistry was first generally confined to a single-step overall reaction $R(c) \rightarrow P(g)$ representing the direct conversion of the condensed (melted) propellant to gaseous products. Generalizations[5,10,11] allowing for a separate (primary) gas flame following the initial multiphase decomposition region were given by $R(c) \rightarrow P(g)$, $R(c) \leftrightarrow R(g)$, $R(g) \rightarrow P(g)$, where $R(g)$ is a gaseous reactant, and by the sequential scheme $R(c) \rightarrow I(g)$, $I(g) \rightarrow P(g)$, where $I(g)$ distinguishes the intermediate gas-phase products from the final products $P(g)$. These schemes were applied to the nonporous case to determine both the structure and propagation velocity of steady, planar nitramine deflagrations, while stability results for these two-phase-flow models have thus far been confined to the case of a single-step mechanism.[6,8,9]

The present work seeks to continue with the analysis of the limiting case in which the primary gas flame intrudes upon the multiphase decomposition region,[10,11] a tendency that is often observed experimentally as the pressure increases. Thus, the single-step case previously analyzed[7] is extended by incorporating both condensed- and gas-phase reactions in the thin multiphase reaction region previously represented by the simple one-step mechanism $R(c) \rightarrow P(g)$. In particular, as indicated above, a global sequential reaction mechanism is assumed, where the first step consists of an overall condensed-phase reaction that produces gas-phase intermediates, and the second step consists of the global reaction of these gas-phase intermediates to produce final gas-phase products. While this simple mechanism is still an extreme approximation to the

actual chemistry that transpires during nitramine deflagration,[12,13] it enables us to fully incorporate two-phase-flow effects into the analysis, and to assess the role of such effects on the structure and propagation of the deflagration in the merged-flame limit just described. The present work complements and extends recent analytical studies of this merged-flame regime[10,11] by computing numerical solutions of the inner reaction-zone eigenvalue problem that may be derived by an asymptotic analysis in the limit of large activation energies. These numerical computations significantly extend the parameter regime that was considered previously, and serve to further characterize the merged-flame limit for these types of problems.

2. The Mathematical Model

We consider the case of an unconfined, steady, planar deflagration, propagating from right to left, into a degraded (porous) energetic solid. Melting of the solid is assumed to occur at a (moving) spatial location $\tilde{x} = \tilde{x}_m(\tilde{t})$ where the solid temperature is equal to the melting temperature $\tilde{T}_m$. Subsequent to melting, gas-phase intermediates are assumed to be produced directly by condensed-phase reactions, and these, in turn, react to form the final combustion products according to

$$R(c) \rightarrow I(g), \quad I(g) \rightarrow P(g), \tag{1}$$

where $R(c)$ denotes the condensed (melted) reactant material, $I(g)$ stands for the intermediate gas-phase species, and $P(g)$ represents the final gas-phase products. The pores within the damaged solid are assumed to be filled with a mixture of the intermediate gas-phase species and final gas-phase products, with the mass-fraction ratio ϕ of the two specified far upstream. The present analysis considers the merged regime in which both reactions occur within a single reaction zone (necessary conditions for which are to be determined), in contrast to a previous (nonporous) study[5] in which these reactions were spatially separated. Thus, the deflagration wave consists of a solid/gas preheat region, the melting surface across which the condensed component of the two-phase mixture undergoes a phase change, a liquid/gas preheat region, a relatively thin (due to the realistic assumption of large activation energies) reaction zone in which all of the condensed-phase material and gas-phase intermediates are converted to gaseous products according to Eq. (1), and finally, the burned region which, in reality, usually corresponds to a dark zone that separates the primary flame region from a secondary gas flame downstream that has little effect on the burning rate.

A reasonable model, appropriate for describing this type of multiphase deflagration wave, was derived previously.[7,10,11] Here, we shall simply state its nondimensional version in a local coordinate system attached to the melting surface $\tilde{x}_m$, with only a brief explanation of the origin of each equation. For simplicity, we restrict our attention to the single-temperature limit of this model, in which case the rates of heat transfer between phases are sufficiently large such that all phases at a given location may be considered to have the same temperature. Thus, before proceeding, we introduce, in terms of dimensional quantities (denoted by tildes), the nondimensional variables

$$x = \frac{\tilde{\rho}_s \tilde{c}_s \tilde{U}}{\tilde{\lambda}_s} \tilde{x}, \quad t = \frac{\tilde{\rho}_s \tilde{c}_s \tilde{U}^2}{\tilde{\lambda}_s} \tilde{t}, \quad T_{s,l,g} = \frac{\tilde{T}_{s,l,g}}{\tilde{T}_u}, \quad u_{l,g} = \frac{\tilde{u}_{l,g}}{\tilde{U}}, \quad \rho_g = \frac{\tilde{\rho}_g}{\tilde{\rho}_g^u}, \tag{2}$$

where the (unknown) propagation speed $\tilde{U} = -d\tilde{x}_m/d\tilde{t}$ is a convenient characteristic velocity for the problem. Here, $\tilde{\rho}$, $\tilde{u}$ and $\tilde{T}$ denote density, velocity and temperature, respectively, and the subscripts s, l and g denote the phase (solid, liquid, gas) to which a quantity refers. For simplicity, constant values for heat capacities

($\tilde{c}$) and thermal conductivities ($\tilde{\lambda}$) are assumed constant for all phases, as are $\tilde{\rho}_s$ and $\tilde{\rho}_l$. In addition, the nondimensional parameters

$$
\begin{aligned}
&r=\frac{\tilde{\rho}_l}{\tilde{\rho}_s}, \quad \hat{r}=\frac{\tilde{\rho}_g^u}{\tilde{\rho}_s}, \quad l=\frac{\tilde{\lambda}_l}{\tilde{\lambda}_s}, \quad \hat{l}=\frac{\tilde{\lambda}_g}{\tilde{\lambda}_s}, \quad b=\frac{\tilde{c}_l}{\tilde{c}_s}, \quad \hat{b}=\frac{\tilde{c}_g}{\tilde{c}_s}, \quad \gamma_s=\frac{\tilde{\gamma}_s}{\tilde{c}_s\tilde{T}_u}, \\
&Le=\frac{\tilde{\lambda}_g}{\tilde{\rho}_g\tilde{D}\tilde{c}_g}, \quad Q_l=\frac{\tilde{Q}_l}{\tilde{c}_s\tilde{T}_u}, \quad Q_g=\frac{\tilde{Q}_g}{\tilde{c}_s\tilde{T}_u}, \quad N_l=\frac{\tilde{E}_l}{\tilde{R}^\circ\tilde{T}_b}, \quad N_g=\frac{\tilde{E}_g}{\tilde{R}^\circ\tilde{T}_b}, \\
&w=\frac{\tilde{W}_I}{\tilde{W}_P}, \quad \Lambda_l=\frac{\tilde{\lambda}_s\tilde{A}_l}{\tilde{\rho}_s\tilde{c}_s\tilde{U}^2}e^{-N_l}, \quad \Lambda_g=\frac{\tilde{\lambda}_s\tilde{A}_g(\tilde{\rho}_g^u)^n}{\tilde{\rho}_s^2\tilde{c}_s\tilde{U}^2}e^{-N_g},
\end{aligned}
\tag{3}
$$

are defined, where n is the reaction order of the gas-phase reaction and Le is the Lewis number associated with the gas phase (having assumed a constant value for $\tilde{\lambda}_g$, we also assume that $\tilde{\rho}_g\tilde{D}$ is constant as well, which implies a constant Lewis number). Here, $\tilde{D}$ is the mass diffusion coefficient and $\tilde{E}$, $\tilde{A}$ and $\tilde{Q}$ denote activation energy, pre-exponential rate coefficient and heat release, respectively, where the subscripts indicate whether these quantities refer to the liquid-phase or the gas-phase reaction. Finally $\tilde{R}^\circ$ is the gas constant, $\tilde{\gamma}_s$ is the heat of melting and $\tilde{W}_I$ and $\tilde{W}_P$ denote the molecular weights of the intermediate and product species, respectively. The subscript or superscript u (*e.g.*, $\tilde{\rho}_g^u$, $\tilde{T}_u$) implies that these quantities are evaluated far upstream in the unburned region. We note that r and $\hat{r}$ are density ratios (liquid-to-solid and upstream gas-to-solid, respectively), l and $\hat{l}$ are thermal conductivity ratios, b and $\hat{b}$ are heat capacity ratios, w is the ratio of molecular weights corresponding to the two gas-phase species, γ_s is a heat-of-melting parameter (negative when melting is endothermic), Q_l and Q_g are heat-release parameters associated with the condensed and gas-phase reactions, respectively, N_l and N_g are the corresponding nondimensional activation energies, and Λ_l and Λ_g are the nondimensional rate coefficients, or Damköhler numbers. Finally, we remark that either Λ_l or Λ_g may be regarded as an appropriate burning-rate eigenvalue, since the determination of either provides an expression for the propagation speed $\tilde{U}$. Indeed, since $\Lambda_g/\Lambda_l=\hat{r}(\tilde{A}_g/\tilde{A}_s)(\tilde{\rho}_g^u)^{n-1}e^{N_l-N_g}$, we shall, for definiteness, regard Λ_l as the burning-rate eigenvalue.

To analyze the case of a steadily propagating deflagration, it is convenient to transform to the moving coordinate $\xi=x+t$ whose origin is defined to be x_m. In the upstream solid/gas region, the volume fraction α of gas is assumed constant ($\alpha=\alpha_s$), and the solid phase is assumed to have constant density and zero velocity (with respect to the laboratory frame of reference). Continuity of the gas phase, on the other hand, is given in the usual fashion by

$$
\frac{d}{d\xi}\left[\rho_g(u_g+1)\right]=0, \quad \xi<0, \tag{4}
$$

$$
\frac{d}{d\xi}\left[\hat{r}\rho_g Y(u_g+1)\right]=\frac{\hat{l}}{\hat{b}}Le^{-1}\frac{d^2Y}{d\xi^2}, \quad \xi<0, \tag{5}
$$

where the first is an overall continuity equation for the gas phase and the latter is the mass conservation equation for the mass fraction Y of the intermediate gas-phase species. In the liquid/gas region to the right of the melting front at $\xi=0$, overall continuity, continuity of the liquid phase, and continuity of the intermediate gas-phase species are given as

$$
\frac{d}{d\xi}\left[r(1-\alpha)(u_l+1)+\hat{r}\alpha\rho_g(u_g+1)\right]=0, \quad \xi>0, \tag{6}
$$

$$
\frac{d}{d\xi}\left[(1-\alpha)(u_l+1)\right]=-\Lambda_l(1-\alpha)\exp\left[N_l\left(1-\frac{T_b}{T_l}\right)\right], \quad \xi>0, \tag{7}
$$

$$\frac{d}{d\xi}\left[\hat{r}\alpha\rho_g Y(u_g+1)+r(1-\alpha)(u_l+1)\right]=\frac{\hat{l}}{\hat{b}}Le^{-1}\frac{d}{d\xi}\left(\alpha\frac{dY}{d\xi}\right)$$
$$-\Lambda_g(\alpha\rho_g Y)^n\exp\left[N_g\left(1-\frac{T_b}{T_g}\right)\right],\quad \xi>0, \tag{8}$$

respectively, where Eq.(7) has been used to eliminate the condensed-phase reaction-rate term that would have otherwise appeared in Eq. (8). Finally, in the single-temperature limit described above, overall energy conservation in the solid/gas and liquid/gas regions is given by

$$(1-\alpha_s)\frac{dT}{d\xi}+\hat{r}\hat{b}\alpha_s\frac{d}{d\xi}\left[\rho_g(u_g+1)T\right]=\frac{d}{d\xi}\left[(1-\alpha_s+\hat{l}\alpha_s)\frac{dT}{d\xi}\right],\quad \xi<0, \tag{9}$$

$$\frac{d}{d\xi}\left[r(1-\alpha)(u_l+1)(Q_l+Q_g+bT)+\hat{r}\alpha\rho_g(u_g+1)(Q_gY+\hat{b}T)\right]$$
$$=\frac{d}{d\xi}\left\{\left[l(1-\alpha)+\hat{l}\alpha\right]\frac{dT}{d\xi}+Q_g\frac{\hat{l}}{\hat{b}}Le^{-1}\alpha\frac{dY}{d\xi}\right\},\quad \xi>0, \tag{10}$$

respectively, where Eqs. (7) and (8) have been used to eliminate the reaction-rate terms that would have otherwise appeared in the latter. We remark that, owing to the assumed smallness of the Mach number, which, for an unconfined deflagration, implies a constant pressure, contributions to Eqs. (9) and (10) that arise from pressure effects are absent.[7]

The above system of equations is closed by adding an equation of state (assumed to be that of an ideal gas) and an expression for the liquid velocity u_l. As indicated above, an approximate analysis of gas-phase momentum conservation implies, for an unconfined, small Mach-number deflagration, that pressure is constant, thereby allowing the equation of state to be expressed as

$$\rho_g T\left[Y+w(1-Y)\right]=\phi+w(1-\phi)\equiv\overline{\phi}, \tag{11}$$

where ϕ is the specified value of Y at $\xi=-\infty$. An analysis of condensed-phase momentum and the assumption of zero velocity for the solid phase, on the other hand, leads to the kinematic approximation

$$u_l=\frac{1}{r}(1-r) \tag{12}$$

in the limit of small viscous and surface-tension-gradient forces.[4,7] Equations (4) – (12) constitute a complete set, which are to be solved subject to the boundary conditions

$$\alpha=\alpha_s \text{ for } \xi\le 0;\quad u_g\to 0,\quad Y\to\phi,\quad T\to 1 \text{ as } \xi\to-\infty, \tag{13}$$

$$\alpha\to 1,\quad Y\to 0,\quad T\to T_b \text{ as } \xi\to+\infty, \tag{14}$$

where $0\le\phi\le 1$, and the melting-surface ($\xi=0$) conditions

$$T|_{\xi=0}=T_m,\quad T\Big|_{\xi=0^-}^{\xi=0^+}=u_g\Big|_{\xi=0^-}^{\xi=0^+}=Y\Big|_{\xi=0^-}^{\xi=0^+}=\frac{dY}{d\xi}\Big|_{\xi=0^-}^{\xi=0^+}, \tag{15}$$

$$\left[l(1-\alpha_s)+\hat{l}\alpha_s\right]\frac{dT}{d\xi}\Big|_{\xi=0^+}-(1-\alpha_s+\hat{l}\alpha_s)\frac{dT}{d\xi}\Big|_{\xi=0^-}=(1-\alpha_s)\left[-\gamma_s+(b-1)T_m\right]. \tag{16}$$

We remark that the final burned temperature T_b is to be determined, as is the burning-rate eigenvalue Λ_l. The latter then determines the propagation velocity of the deflagration according to its definition given in Eq. (3), and is the main result to be determined from the analysis that follows.

3. Determination of T_b and $u_{g,\infty}$

The solution in the region $\xi < 0$, where chemical activity has been assumed to be absent, as well as expressions for T_b and $u_{g,\infty} \equiv u_g\big|_{\xi=\infty}$, are obtained from the above model as follows. From Eqs. (4) and (13), we have

$$\rho_g(u_g + 1) = 1\,, \quad \xi < 0\,, \tag{17}$$

while an integration of Eq. (5) gives, upon use of Eq. (17), the integral

$$Y - \phi = \frac{\hat{l}}{\hat{r}\hat{b}} Le^{-1} \frac{dY}{d\xi}\,, \quad \xi < 0\,. \tag{18}$$

Similarly, integrating Eq. (6) implies

$$(1-\alpha) + \hat{r}\alpha\rho_g(u_g + 1) = \hat{r}\rho_g^b(u_{g,\infty} + 1)\,, \quad \xi > 0\,, \tag{19}$$

where $\rho_g^b = (wT_b)^{-1}$ is the burned gas density. Thus, evaluating Eq. (19) at $\xi = 0$ using Eq. (17) and the fact that all variables are continuous there, an expression for the burned gas velocity $u_{g,\infty}$ is obtained as

$$u_{g,\infty} = \frac{1 + \alpha_s(\hat{r} - 1)}{\hat{r}\rho_g^b} - 1 = \frac{1 + \alpha_s(\hat{r} - 1)}{\hat{r}\overline{\phi}} wT_b - 1\,. \tag{20}$$

Turning attention to the overall energy equations (9) and (10), we may readily perform a single integration on each using the preceding results to obtain

$$(1 - \alpha_s + \hat{r}\hat{b}\alpha_s)(T - 1) = (1 - \alpha_s + \hat{l}\alpha_s)\frac{dT}{d\xi}\,, \quad \xi < 0 \tag{21}$$

and

$$\begin{aligned} &\left[b(1-\alpha) + \hat{b}(\alpha - \alpha_s + \alpha_s\hat{r})\right] T + (\alpha - \alpha_s + \alpha_s\hat{r})Q_g Y \\ &\quad = \left[l(1-\alpha) + \hat{l}\alpha\right] \frac{dT}{d\xi} + Q_g \frac{\hat{l}}{\tilde{b}} Le^{-1}\alpha \frac{dY}{d\xi} - (1-\alpha)(Q_l + Q_g) + \hat{b}(1 - \alpha_s + \alpha_s\hat{r})T_b\,, \quad \xi > 0\,, \end{aligned} \tag{22}$$

Thus, subtracting Eq. (21) evaluated at $\xi = 0^-$ from Eq. (22) evaluated at $\xi = 0^+$ and using the melting-surface conditions (15) and (16), we derive for T_b the expression

$$T_b = \frac{(1-\alpha_s)(Q_l + Q_g + 1 + \gamma_s) + \hat{r}\alpha_s(\phi Q_g + \hat{b})}{\hat{b}\,[1 + \alpha_s(\hat{r} - 1)]}\,. \tag{23}$$

We note that this identical result can be derived from a more general two-temperature model[10] and is independent of the particular form of the equation of state for the gas. In the limit $Q_g \to 0$, Eq. (23) collapses to the result obtained for the corresponding single-step model analyzed previously.[7] Equations (18), (21) and (22), which are first integrals of Eqs. (5), (9) and (10), now take the place of the latter in our model.

We note that there are significant variations of the final burned temperature and gas velocity with pressure, since these quantities depend on the upstream gas-to-solid density ratio $\hat{r}$, which in turn is proportional to the pressure $\tilde{p}_g^\circ$ according to $\hat{r} \equiv \tilde{\rho}_g^u/\tilde{\rho}_s = \tilde{W}_I\tilde{p}_g^\circ/\tilde{\rho}_s\tilde{R}^\circ\tilde{T}_u\overline{\phi}$. As discussed previously,[7] this important effect arises from the thermal expansion of the gas and the two-phase nature of the flow in the solid/gas and

liquid/gas regions, where significant gas-phase convective transport of enthalpy relative to the condensed phase occurs. In the limit $\tilde{p}_g^\circ \to 0$ (*i.e.*, $\hat{r} \to 0$), we see that $u_{g,\infty} \to \infty$ and $T_b \to T_b^0 \equiv \hat{b}^{-1}(Q_l + Q_g + 1 + \gamma_s)$. Since there is effectively no gas-phase enthalpy content in this limit, T_b^0 is also the value of T_b in the limit of zero porosity ($\alpha_s \to 0$). For nonzero values of both pressure and porosity, some of the heat released by combustion must be used to help raise the temperature of the gas-phase intermediates within the porous solid from unity to T_b. Consequently, both T_b and the final gas velocity $u_{g,\infty}$ are typically decreasing functions of the nondimensional gas-phase density $\hat{r}$, which increases with pressure according to the above relation. An additional effect that is revealed by the two-step reaction mechanism is that T_b does not depend just on the total heat release $Q_l + Q_g \equiv Q$ associated with the complete conversion of the energetic solid to final gas products, but also on the heat release Q_g specifically associated with the gas-phase reaction. This, too, is a two-phase-flow effect that arises from the fact that the reactive intermediate gas-phase species occupy the voids in the porous solid, and the heat released by these pre-existing intermediates affects the final burned temperature. In particular, for a given total heat release Q, the burned temperature increases as the fractional heat release associated with the gas-phase reaction increases.

4. The Asymptotic Limit and the Outer Solution

Further analytical development, leading to the determination of the burning-rate eigenvalue Λ_l, requires an analysis of the reactive liquid/gas region $\xi > 0$. Equations (7), (8) and (22) constitute three equations for Y, T and α in this region, with u_g then determined from Eq. (19) along with the equation of state (11), and the eigenvalue Λ_l determined by the boundary conditions. In order to handle the Arrhenius nonlinearities in Eqs. (7) and (8), we exploit the largeness of the nondimensional activation energies N_g and N_l, and consider the formal asymptotic limit N_g, $N_l \gg 1$ such that

$$\frac{N_g}{N_l} = \nu\,, \quad \beta \equiv (1 - T_b^{-1})N_l \gg 1\,, \tag{24}$$

where ν is an O(1) parameter and the Zel'dovich number β is the large activation-energy parameter that naturally emerges in the analysis that follows. For simplicity, we shall eventually assume $\nu \approx 1$, in which case Eq. (24) implies that we are considering the regime in which the two large activation energies differ by an approximately O(1) amount. The relation (24), along with a corresponding order relation for the ratio Λ_g/Λ_l to be introduced shortly, helps to insure that both the condensed and gas-phase reactions are active in a single thin reaction zone. Departures from Eq. (24) allow for separated reaction zones,[5] but in the present work we shall focus on the merged case just described.

In the limit $\beta \to \infty$, the Arrhenius terms are exponentially small unless T is within $O(1/\beta)$ of T_b. Consequently, all chemical activity is concentrated in a very thin reaction zone whose thickness is $O(1/\beta)$. On the scale of the (outer) coordinate ξ, this thin region is a sheet whose location is denoted by $\xi_r = x_r - x_m$, where $x_r > x_m$. Hence, the semi-infinite liquid/gas region is comprised of a preheat zone ($0 < \xi < \xi_r$) where chemical activity is exponentially small, the thin reaction zone where the two chemical reactions are active and go to completion, and a burned region $\xi > \xi_r$. Denoting the outer solutions on either side of the reaction zone by a zero superscript, we conclude from Eq. (7) that

$$\alpha^0 = \begin{cases} \alpha_s\,, & \xi < \xi_r\,, \\ 1\,, & \xi > \xi_r\,, \end{cases} \tag{25}$$

and from Eqs. (11), (17), (19) and (20),

$$u_g + 1 = \frac{\alpha - \alpha_s + \hat{r}\alpha_s}{\hat{r}\alpha\bar{\phi}}\,[Y + w(1 - Y)]\,T \tag{26}$$

for all ξ. We observe that there is a jump in α^0, and hence also in u_g^0, across the reaction zone. Similarly, in obtaining the complete outer solution for Y and T, it is necessary to connect the solutions on either side of the reaction zone by deriving appropriate jump conditions across $\xi = \xi_r$. This will ultimately entail the introduction of a stretched coordinate (see below) appropriate for analyzing the inner structure within the reaction zone, whereupon an asymptotic matching of the inner and outer solutions will yield not only the aforementioned jump conditions, but also the burning-rate eigenvalue as well. In connection with this procedure, it is convenient, and physically appealing, to attempt a representation of the reaction-rate terms in Eqs. (7) and (8) as delta-function distributions with respect to the outer spatial variable ξ.[10,11] As a result, using the results (25) and (26), the governing system of equations for the outer solution variables Y^0 and T^0 become

$$\hat{r}(Y^0 - \phi) = \frac{\hat{l}}{\hat{b}} Le^{-1} \frac{dY^0}{d\xi}, \quad \xi < 0, \tag{27}$$

$$\frac{d}{d\xi}\left[(\alpha^0 - \alpha_s + \hat{r}\alpha_s)Y^0 - \alpha^0\right] = \frac{\hat{l}}{\hat{b}} Le^{-1} \frac{d}{d\xi}\left(\alpha^0 \frac{dY^0}{d\xi}\right) - P_g \delta(\xi - \xi_r - H), \quad \xi > 0, \tag{28}$$

$$\frac{1}{r}\frac{d\alpha^0}{d\xi} = P_l \delta(\xi - \xi_r), \quad \xi > 0, \tag{29}$$

$$(1 - \alpha_s + \hat{r}\hat{b}\alpha_s)(T^0 - 1) = (1 - \alpha_s + \hat{l}\alpha_s)\frac{dT^0}{d\xi}, \quad \xi < 0, \tag{30}$$

and

$$\begin{aligned}\left[b(1-\alpha^0) + \hat{b}(\alpha^0 - \alpha_s + \alpha_s\hat{r})\right] T^0 + (\alpha^0 - \alpha_s + \alpha_s\hat{r})Q_g Y^0 = \left[l(1-\alpha^0) + \hat{l}\alpha^0\right]\frac{dT^0}{d\xi} \\ + Q_g \frac{\hat{l}}{\hat{b}} Le^{-1}\alpha^0 \frac{dY^0}{d\xi} - (1-\alpha^0)(Q_l + Q_g) + \hat{b}(1 - \alpha_s + \alpha_s\hat{r})T_b, \quad \xi > 0,\end{aligned} \tag{31}$$

where P_l and P_g are the source strengths of the reaction-rate distributions placed at $\xi = \xi_r$ and $\xi = \xi_r + H$, respectively. These quantities, along with the separation constant H, are to be determined, where the ability to do so validates the delta-function representation of the reaction rates, at least to the order of analysis considered here. We note that the $O(1/\beta)$ width of the merged reaction zone implies that H is of this order (or smaller) as well, and in fact we will eventually seek H as an expansion in inverse powers of β.

The solution of Eqs. (27) – (31) subject to the melting conditions at $\xi = 0$ and the boundary conditions at $\xi = \pm\infty$ is straightforward and given by

$$P_l = \frac{1}{r}(1 - \alpha_s), \quad P_g = 1 - \alpha_s + \hat{r}\alpha_s\phi, \tag{32}$$

$$Y^0(\xi) = \begin{cases} \phi + \left\{\dfrac{(1-\phi)(1-\alpha_s)}{1-\alpha_s+\hat{r}\alpha_s} - \dfrac{1-\alpha_s+\hat{r}\alpha_s\phi}{1-\alpha_s+\hat{r}\alpha_s}\exp\left[-(1-\alpha_s+\hat{r}\alpha_s)\hat{b}LeH/\hat{l}\right]\right\} \\ \qquad\qquad \times \exp\left[\hat{r}\hat{b}Le(\xi - \xi_r)/\hat{l}\right], & \xi < \xi_r, \\ \dfrac{1-\alpha_s+\hat{r}\alpha_s\phi}{1-\alpha_s+\hat{r}\alpha_s}\left\{1 - \exp\left[(1-\alpha_s+\hat{r}\alpha_s)\hat{b}Le(\xi - \xi_r - H)/\hat{l}\right]\right\}, & \xi_r < \xi < \xi_r + H, \\ 0, & \xi > \xi_r + H, \end{cases} \tag{33}$$

$$T^0(\xi) = \begin{cases} 1 + (T_m - 1)\exp\left[\dfrac{1-\alpha_s+\hat{r}\hat{b}\alpha_s}{1-\alpha_s+\hat{l}\alpha_s}\xi\right], & \xi < 0, \\ B + (T_m - B)\exp\left[\dfrac{b(1-\alpha_s)+\hat{r}\hat{b}\alpha_s}{l(1-\alpha_s)+\hat{l}\alpha_s}\xi\right], & 0 < \xi < \xi_r, \\ B_1 + (T_b - B_1)\exp\left[\dfrac{\hat{b}}{\hat{l}}(1-\alpha_s+\hat{r}\alpha_s)(\xi-\xi_r-H)\right], & \xi_r < \xi < \xi_r + H, \\ T_b = B_1 + \dfrac{1-\alpha_s+\hat{r}\alpha_s\phi}{\hat{b}(1-\alpha_s+\hat{r}\alpha_s)}Q_g, & \xi > \xi_r + H, \end{cases} \tag{34}$$

where

$$B \equiv \frac{(1-\alpha_s)(1+\gamma_s)+\hat{r}\hat{b}\alpha_s}{b(1-\alpha_s)+\hat{r}\hat{b}\alpha_s}, \quad B_1 \equiv \frac{(1-\alpha_s)(Q_l+1+\gamma_s)+\hat{r}\hat{b}\alpha_s}{\hat{b}(1-\alpha_s+\hat{r}\alpha_s)}. \tag{35}$$

The location ξ_r of the reaction zone, which appears as a sheet on the scale of the outer variable ξ, is thus determined by Eq. (34) from continuity of T at $\xi = H$ as

$$\xi_r = \frac{l(1-\alpha_s)+\hat{l}\alpha_s}{b(1-\alpha_s)+\hat{r}\hat{b}\alpha_s} \ln\left\{\frac{B_1 - B + (T_b - B_1)\exp\left[-\hat{b}(1-\alpha_s+\hat{r}\alpha_s)H/\hat{l}\right]}{T_m - B}\right\}. \tag{36}$$

A sketch of the outer solution is shown in Figure 1 for $\phi = 1$ and typical values of the remaining parameters.

We remark that since $H \lesssim O(1/\beta)$ in magnitude, the interval $\xi_r < \xi < H$ lies within the merged reaction zone, which, on the scale of the outer coordinate ξ, is a sheet at $\xi = \xi_r$. Consequently, that portion of Eqs. (33) and (34) that actually represents the outer solution is the solution for $\xi < \xi_r^- = \min(\xi_r, \xi_r + H)$ and $\xi > \xi_r + H \approx \xi_r^+$, where (small) H may be either positive or negative. Thus, Eqs. (33) and (34) imply an $O(1/\beta)$ jump in the outer solutions Y^0 and T^0 across the reaction zone. This can be motivated directly by noting that for H small, an expansion of the delta-function $\delta(\xi - \xi_r - H)$ in Eq. (28) about $H = 0$ introduces the derivative of the delta-function, $\delta'(\xi - \xi_r)$,14, 15 where the latter implies a higher order singularity (discontinuities in the variables Y^0 and T^0 themselves) at $\xi = \xi_r$ than that which occurs when H is identically zero. The actual values of these discontinuities, as determined here by the value of the separation constant H, as well as the burning-rate eigenvalue Λ_l, are calculated by matching the above outer solution to the inner solution of the reaction-zone problem, which we now consider.

5. The Reaction-Zone Problem

To analyze the chemical boundary layer that lies in the vicinity of ξ_r, we introduce a stretched inner variable η and a normalized temperature variable Θ defined by

$$\eta = \beta(\xi - \xi_r), \quad \Theta = \frac{T-1}{T_b - 1}, \tag{37}$$

where the Zel'dovich number $\beta \gg 1$ was defined by the second of Eqs. (24). We then seek solutions in the form of the expansions

$$\begin{aligned} &\alpha \sim \alpha_0 + \beta^{-1}\alpha_1 + \beta^{-2}\alpha_2 + \cdots, \quad u_g \sim u_0 + \beta^{-1}u_1 + \beta^{-2}u_2 + \cdots, \\ &Y \sim \beta^{-1}y_1 + \beta^{-2}y_2 + \cdots, \quad \Theta \sim 1 + \beta^{-1}\theta_1 + \beta^{-2}\theta_2 + \cdots, \\ &\Lambda_l \sim \beta(\Lambda_0 + \beta^{-1}\Lambda_1 + \beta^{-2}\Lambda_2 + \cdots), \quad H \sim \beta^{-1}h_1 + \beta^{-2}h_2 + \cdots, \end{aligned} \tag{38a}$$

where the coefficients in the expansion of u_g are calculated in terms of the α_i, y_i and θ_i from Eq. (26), which is also valid in the reaction zone. At this point, we also order the nondimensional rate-coefficient ratio Λ_g/Λ_l as

$$\frac{\Lambda_g}{\Lambda_l} = \hat{r}(\tilde{\rho}_g^u)^{n-1}\frac{\tilde{A}_g}{\tilde{A}_l}\exp[(1-\nu)N_l] \equiv \beta^n\lambda\,, \tag{38b}$$

where ν is the activation-energy ratio defined by the first of Eqs. (24) and λ is an analogous O(1) parameter that defines the scaled value of the rate-coefficient ratio. The scaling embodied in Eq. (38b) is required, given Eq. (24), to construct an inner solution that corresponds to a merged reaction zone. As discussed below Eq. (24), different scalings are permissible, but would generally correspond to separated reaction zones for the condensed and gas-phase reactions.[5]

Substituting the above inner expansions into Eqs. (7), (8) and (22), the governing equations for the leading-order inner variables α_0, y_1 and θ_1 are given by

$$\frac{d\alpha_0}{d\eta} = r\Lambda_0(1-\alpha_0)\,e^{\theta_1}\,, \tag{39}$$

$$\left[l + (\hat{l}-l)\alpha_0\right]\frac{d\theta_1}{d\eta} + \frac{\hat{l}Q_g}{\hat{b}Le(T_b-1)}\alpha_0\frac{dy_1}{d\eta} = \frac{(b-\hat{b})T_b + Q_l + Q_g}{T_b-1}(1-\alpha_0)\,, \tag{40}$$

$$\frac{\hat{l}}{\hat{b}}Le^{-1}\frac{d}{d\eta}\left(\alpha_0\frac{dy_1}{d\eta}\right) = -\frac{d\alpha_0}{d\eta} + \lambda\left(\frac{\overline{\phi}}{wT_b}\right)^n\Lambda_0(\alpha_0 y_1)^n e^{\nu\theta_1}\,. \tag{41}$$

Solutions to these inner equations as $\eta \to \pm\infty$ must match with the outer solution (25), (33) and (34) as $\xi \uparrow \xi_r^-$ and as $\xi \downarrow (\xi_r + H)^+$, respectively. This leads to the matching conditions

$$\alpha_0 \to 1\,, \quad \theta_1 \to 0\,, \quad y_1 \to 0 \text{ as } \eta \to +\infty\,, \tag{42}$$

$$\alpha_0 \to \alpha_s\,, \quad \theta_1 \sim E_1\eta + E_2 h_1\,, \quad y_1 \sim \frac{\hat{b}}{\hat{l}}Le\left[-\hat{r}\eta + (1-\alpha_s+\hat{r}\alpha_s\phi)h_1\right] \text{ as } \eta \to -\infty\,, \tag{43}$$

where the coefficients E_1 and E_2 in the second of Eqs. (43) are defined as

$$E_1 = \frac{T_b - B}{T_b - 1}\cdot\frac{b(1-\alpha_s)+\hat{r}\hat{b}\alpha_s}{l(1-\alpha_s)+\hat{l}\alpha_s}\,, \qquad E_2 = -\frac{T_b - B_1}{T_b - 1}\cdot\frac{\hat{b}}{\hat{l}}(1-\alpha_s+\hat{r}\alpha_s)\,. \tag{44}$$

Solution of the complete inner problem given by Eqs. (39) – (44) will only be possible for certain values of h_1 and Λ_0, where the latter is the scaled leading-order coefficient in the expansion of the burning rate eigenvalue. We note that Eqs. (39) – (41) may be simplified somewhat by employing α_0 as the independent variable. Thus, using Eq. (39), Eqs. (40) and (41) may be written as

$$\left[l + (\hat{l}-l)\alpha_0\right]e^{\theta_1}\frac{d\theta_1}{d\alpha_0} + \frac{\hat{l}Q_g}{\hat{b}Le(T_b-1)}\alpha_0 e^{\theta_1}\frac{dy_1}{d\alpha_0} = \frac{(b-\hat{b})T_b + Q_l + Q_g}{(T_b-1)r\Lambda_0}\,, \tag{45}$$

$$r\Lambda_0\frac{\hat{l}}{\hat{b}}Le^{-1}\frac{d}{d\alpha_0}\left[\alpha_0(1-\alpha_0)e^{\theta_1}\frac{dy_1}{d\alpha_0}\right] = -1 + \frac{\lambda}{r}\left(\frac{\overline{\phi}}{wT_b}\right)^n\frac{(\alpha_0 y_1)^n}{1-\alpha_0}e^{(\nu-1)\theta_1}\,. \tag{46}$$

Although a closed-form solution to this system is not readily apparent, further analytical development may proceed through a perturbation analysis of Eqs. (45) and (46) in the limit that Q_g is small relative to Q_l,[10,11] which, to leading order, decouples Eq. (46) from Eq. (45). This limit corresponds to the assumption that most of the heat release occurs in the first stage of the two-step reaction process, which realistically

implies that at least some of the initial exothermic gas-phase decomposition reactions should be lumped with the overall reaction (1a), regarding the resulting decomposition products as the gas-phase intermediates $I(g)$. This analysis is summarized in the Appendix. Here, we avoid any further approximations by seeking numerical solutions of the double eigenvalue problem (39) – (43), thereby greatly expanding the parameter regime to which our previous analytical analysis was restricted.

6. Computational Procedure

The numerical solution of Eqs. (39) – (43) is facilitated by rewriting Eqs. (39) – (41) as a first-order system and introducing trivial equations for the eigenvalues Λ_0 and h_1. We thus obtain the equivalent problem

$$\frac{d\alpha_0}{d\eta} = r\Lambda_0(1-\alpha_0)\,e^{\theta_1}\,, \tag{47}$$

$$\frac{d\theta_1}{d\eta} = \frac{1}{l+(\hat{l}-l)\alpha_0}\left[\frac{(b-\hat{b})T_b+Q_l+Q_g}{T_b-1}(1-\alpha_0^0) - \frac{\hat{l}Q_g}{\hat{b}Le(T_b-1)}\alpha_0\frac{dy_1}{d\eta}\right], \tag{48}$$

$$\frac{dy_1}{d\eta} = \frac{z}{\alpha_0}\,, \tag{49}$$

$$\frac{dz}{d\eta} = -\frac{\hat{b}Le}{\hat{l}}\left[\frac{d\alpha_0}{d\eta} - \lambda\Lambda_0\left(\frac{\overline{\phi}}{wT_b}\right)^n(\alpha_0 y_1)^n e^{\nu\theta_1}\right], \tag{50}$$

$$\frac{d\Lambda_0}{d\eta} = \frac{dh_1}{d\eta} = 0\,, \tag{51}$$

subject to Eq. (42) as $\eta \to +\infty$ and

$$\alpha_0 \to \alpha_s\,, \quad \theta_1 + \frac{\hat{l}E_1}{\hat{r}\hat{b}Le}y_1 \sim \left[E_2 + \frac{E_1}{\hat{r}}(1-\alpha_s+\hat{r}\alpha_s)\right]h_1\,, \quad z \sim -\frac{\alpha_s\hat{r}\hat{b}Le}{\hat{l}} \text{ as } \eta \to -\infty\,, \tag{52}$$

where the boundary (matching) conditions as $\eta \to -\infty$ have been reformulated so as to make the problem invariant with respect to the choice of origin for the independent variable η. Equations (47) – (51) constitute a system of six first-order equations, subject to the six boundary conditions embodied in Eqs. (47) and (52), for the six unknowns α_0, θ_1, y_1, z, Λ_0 and h_1. Thus, solution of this well-posed problem will determine the eigenvalues Λ_0 and h_1.

The above problem represents a nonlinear coupled boundary-value problem on a doubly infinite domain. Accurate numerical solutions may be obtained on an approximate finite domain provided internal boundary conditions are imposed on one of the variables to ensure that the reaction zone will be positioned well into the interior of the domain. Since Eqs. (47) – (51) and the boundary conditions (42) and (52) are independent of the choice of origin, this can be achieved without loss of generality by specifying a value of one of the variables (*e.g.*, the volume fraction α) at $\eta = 0$. Then, the computational domain may be divided in half and a new set of variables introduced for one half of the domain. That part of the domain is then mapped onto the other half and additional continuity conditions specified for the two corresponding sets of variables at $\eta = 0$.[16]

The numerical code used in our computations was the routine TWPBVP,[17–20] which handles an arbitrary system of first-order equations provided all boundary conditions are imposed at the external boundaries of the computational domain. Partitioning the domain as described above, we thus end up with a system

of twelve first-order equations for the two sets of six variables in each of the two subdomains that are now mapped onto one another. The numerical method itself is an iterative deferred-correction scheme based on mono-implicit Runge-Kutta formulas with adaptive mesh refinement. In order to achieve convergence, a nontrivial initial guess was required. The solutions obtained from the perturbation analysis summarized in the Appendix proved to be adequate in almost all cases. In those instances when the initial guess obtained from the perturbation analysis was not sufficient, a continuation approach based on the previous iterated solution for a nearby set of parameter values was used. The computational domain was approximated by $-40 \leq \eta \leq 40$, where the endpoints were determined to correspond to the points at which double precision resolution breaks down for this problem [*e.g.*, $\alpha_0(\eta = 40) = 1$ to double-precision accuracy on a Sun 10 workstation]. The initial grid was composed of 500 equidistant points, which was usually sufficient to obtain convergence given an absolute tolerance of 10^{-6} on all variables.

7. Discussion of Results

The solution structure of the dependent variables as a function of η, and the numerical values of the eigenvalues Λ_0 and h_1, are exhibited in Figure 2 for a set of parameter values consistent with the analytical solution obtained previously[10,11] (see Appendix). It is thus seen that there is reasonably good agreement between the numerical and analytical solutions in the parameter regime where the latter is valid. The only modest differences are in the profiles for y_1 and h_1, which stem from the fact that the analytical expressions for these quantities are not calculated to the same order of accuracy as α_0, θ_1 and Λ_0 (one-term versus two-term expansions), as indicated in the Appendix. We have also observed that the numerical value of h_1 is a relatively sensitive function of the system parameters, which may also account for the relatively minor discrepancies evident in Figure 2. The main computational results are given in Figures 3 – 11, where Figures 3a – 11a show the behavior of the burning-rate eigenvalue Λ_0, which is related to the dimensional propagation speed $\tilde{U}$ according to the penultimate of Eqs. (3) [see Eqs. (38a) and (24)], and the separation eigenvalue h_1 as a function of α_s. Figures 3b – 11b show plots of the corresponding unscaled dimensional quantities $\tilde{U}$ and $\tilde{H} = (\tilde{\lambda}_s/\tilde{\rho}_s\tilde{c}_s\tilde{U})h_1/\beta$, where the latter follows from the dimensional version of H and the last of Eqs. (38a). A set of base values for the parameters was adopted, and each figure shows the effect of varying one of these parameters (as a function of α_s), while keeping the remaining parameters fixed. The numerical computations were performed for values of α_s ranging from 0.01 to 0.9.

It is readily seen that Λ_0 and h_1 are generally decreasing functions of the porosity α_s of the solid. We note, however, that although the dimensional propagation speed $\tilde{U}$ is inversely proportional to $1/\sqrt{\Lambda_0}$ according to the definition of Λ_0, it is also proportional to e^{-N_t}, which decreases with increasing porosity due to a decrease in the burned temperature T_b. The exponential sensitivity of $\tilde{U}$ to the latter implies that this thermodynamic effect usually will dominate, and hence $\tilde{U}$ will generally be a decreasing function of α_s as well. In a similar vein, we observe that although h_1 is a monotonically decreasing function of α_s, its unscaled dimensional counterpart $\tilde{H}$ is also inversely proportional to $\tilde{U}$ and the Zel'dovich number β, both of which are decreasing functions of α_s as noted above. Consequently, $\tilde{H}$ frequently exhibits a local maximum due to changes in the relative rates of decrease of h_1 and $\beta\tilde{U}$ as α_s increases. In particular, we note that the slope of h_1 tends to be relatively large in magnitude for small and large α_s and relatively small for intermediate values of α_s. Hence, $\tilde{H}$ tends to be a decreasing function in the former regions, and an increasing function in the latter, where the increasing behavior of $1/\beta\tilde{U}$ causes $\tilde{H}$ to increase with α_s as well. We remark that as α_s approaches either zero or unity, the absolute value of h_1 often becomes large, indicating a breakdown of

the merged-flame solution due to increasing separation between the effective location of the condensed and gas-phase reactions.

The behavior of $h_1(\alpha_s)$ is especially sensitive to the value of the upstream gas-to-solid density ratio $\hat{r}$ as $\hat{r}$ decreases (Figure 3a). In the limit of small α_s, only increasingly larger values of $\hat{r}$ are consistent with a merged-flame solution, since otherwise there is a tendency for the gas-phase reaction to either occur increasingly downstream of the gas-phase reaction, corresponding to blow-off ($h_1 \to \infty$), or for gas-phase reaction of the intermediates initially present within the porous solid to occur upstream within the two-phase region ($h_1 \to -\infty$). The former result is consistent with the analytical analysis for small Q_g and α_s (as discussed in the last paragraph of the Appendix), but both trends are attributable to the sensitivity of the merged-flame structure to the amount of gas-phase convective transport relative to the condensed material (since smaller values of $\hat{r}$ result in larger gas-phase velocities [*cf.* Eq. (20)]. We note that for fixed α_s, the dimensional burning rate $\tilde{U}$ increases with decreases in the parameter $\hat{r}$, and that for small values of $\hat{r}$, the value of $\tilde{U}$ can, in spite of the argument given above, actually increase with α_s until α_s becomes sufficiently large (Figure 3b). This behavior is due to the fact that the decrease in T_b with increasing α_s is diminished for decreasing values of $\hat{r}$, so that T_b, and thus β, vary little with α_s in the limit of small gas-phase density until α_s approaches unity. Consequently, as α_s increases from zero, the behavior of $\tilde{U}^2$ is approximately inversely proportional to Λ_0 until changes in T_b due to increasing values of the porosity become sufficiently large to counteract this trend, as discussed above.

Various other effects that are readily apparent are the decrease in h_1 and Λ_0 (and the corresponding increase in U) with increasing values of the gas-to-solid rate-ratio parameter λ (Figure 4), with a similar trend observed for the changes in these quantities as the Lewis number increases (Figure 5). The behavior with respect to changes in λ corresponds to an increasing rate for the gas-phase reaction relative to the condensed step, so it is clear that the separation constant should decrease as λ increases, and that for fixed values of the condensed reaction rate, the propagation speed should increase. In a similar vein, increasing the Lewis number by decreasing the mass diffusivity of the gas relative to its thermal diffusivity results in a higher concentration of the reactive intermediate gas species in the reaction zone, resulting in a faster burning rate.

The effect of varying the relative heat release attributable to each of the two reactions is shown in Figure 6, where variations in the nondimensional gas-phase heat release Q_g are accompanied by variations in the corresponding liquid-phase parameter Q_l such that the total heat release $Q \equiv Q_g + Q_l$ remains constant. Nonetheless, according to Eq. (23), the burned temperature T_b continues to increase with increasing Q_g, resulting in a critical value of α_s above (below) which the burning rate $\tilde{U}$ increases (decreases) with increasing Q_g. A plausible explanation for this effect is that the accompanying decrease in Q_l tends to slow the rate of the condensed reaction, which essentially defines the burning rate, but the resulting increase in overall burned temperature tends to compensate for this effect. As α_s increases from small values, the decreasing scaled separation h_1 between the condensed and gas-phase reactions can thus produce a corresponding increase in temperature in the vicinity of the condensed reaction. At the critical value of α_s, this overall thermal effect completely compensates for the effect of decreasing Q_l. Hence, for α_s above this value, the latter effect dominates and the burning rate thus increases with increasing Q_g.

Another interesting effect is associated with increases in the upstream intermediate-to-product mass-fraction ratio ϕ (Figure 7). In particular, although a decrease in the upstream mass fraction of intermediates produces relatively little effect on the burning rate, the separation distance between the condensed and gas-phase reactions is highly sensitive to changes in this parameter, especially for larger values of α_s. As ϕ decreases, larger values of α_s are increasingly inconsistent with a merged-flame solution, since it requires the

gas-phase reaction to preheat the condensed material to compensate for the decrease in T_b with decreasing ϕ_s. As ϕ_s continues to decrease, there are less and less unburned intermediates in the upstream region to accomplish this preheating, and the gas-phase reaction must therefore shift further and further upstream relative to the condensed reaction to compensate for the reduced amount of preheating. This preheating effect also explains the decrease in burning rate for decreasing values of the gas-to-solid thermal conductivity ratio $\hat{l}$ (Figure 8). This reduces the amount of gas-phase diffusive heat transport from the burned to the unburned regions, and the compensating necessity of having the gaseous reaction move closer, and ultimately upstream, of the condensed reaction (as α_s increases) so as to produce a sufficient amount of condensed-phase preheating. This latter result is also consistent with the analytical predictions for small Q_g and α_s.[10,11]

Finally, we note that the burning rate increases with decreasing values of the gas-to-solid heat capacity ratio $\hat{b}$ (Figure 9), since larger gas-phase heat capacities require a greater proportion of the heat released by chemical reaction to warm the pre-existing burned products in the upstream region to the final burned temperature. We also observe that the scaled separation of the condensed and gas-phase reactions is sensitive to variations in the ratio ν of activation energies (Figure 10). In particular, as the activation energy of the gas-phase reaction increases relative to that of the condensed reaction, its reaction rate decreases and consequently, the separation of the two reactions increases and the burning rate decreases, consistent with the behavior obtained for decreasing λ, as described above. A similar effect is observed with respect to increases in the gas-phase reaction order n (Figure 11).

In summary, it is clear that although not all parameter values are consistent with a merged-flame structure, there is a well-defined regime that supports this type of deflagration in which condensed-phase decomposition and the primary gas flame merge in a single multiphase reaction zone. In particular, consistent with experiments involving nitramine propellants such as HMX and RDX that generally show the primary gas flame approaching the propellant surface as the pressure (and hence density) increases, we find that O(1) values of the gas-to-solid density ratio and/or the porosity support such a structure for reasonable combinations of values for the remaining parameters. This particular parameter regime is thus one in which convective gas-phase transport, as reflected by the expression for u_g^b given in Eq. (12), relative to the condensed material is sufficiently reduced to permit both types of reactions to occur in the same spatial zone. As $\hat{r}$ and/or α_s decrease, u_g^b increases to the point that the gas-phase reaction is pushed downstream, leading to separated reaction zones.

Appendix. Perturbation Solutions for Small Q_g

As indicated below Eq. (46), an analytical solution of the reaction-zone problem may be obtained as a perturbation expansion for small values of Q_g.[10,11] Since this solution is useful as an initial guess in obtaining the numerical solutions described in Sections 6 and 7, we summarize these results here. Thus, we formally introduce a small bookkeeping parameter ϵ, where $O(\beta^{-1}) \ll \epsilon \ll O(1)$, and write $Q_g = \epsilon Q_g^1$, where $Q_g^1 \sim O(1)$. We may now seek solutions to the leading-order inner problem in the form

$$\begin{gathered}\alpha_0 \sim \alpha_0^0 + \epsilon\alpha_0^1 + \epsilon^2\alpha_0^2 + \cdots, \quad y_1 \sim y_1^0 + \epsilon y_1^1 + \epsilon^2 y_1^2 + \cdots, \quad \theta_1 \sim \theta_1^0 + \epsilon\theta_1^1 + \epsilon^2\theta_1^2 + \cdots, \\ \Lambda_0 \sim \Lambda_0^0 + \epsilon\Lambda_0^1 + \epsilon^2\Lambda_0^2 + \cdots, \quad h_1 \sim h_1^0 + \epsilon h_1^1 + \epsilon^2 h_1^2 + \cdots.\end{gathered} \tag{A.1}$$

Substituting these latest expansions into Eqs. (45) and (46), it is readily seen that a subproblem for α_0^0 and θ_1^0 decouples from the full leading-order problem (with respect to ϵ), and that it is identical in form

to that obtained for the single-step analysis corresponding to the global reaction scheme $R(c) \to P(g)$.[7] In particular, we obtain from Eqs. (39) and (45)

$$\left[l + (\hat{l} - l)\alpha_0^0\right] e^{\theta_1^0} \frac{d\theta_1^0}{d\alpha_0^0} = \frac{(b - \hat{b})B_1 + Q_l}{(B_1 - 1)r\Lambda_0^0}, \quad \frac{d\alpha_0^0}{d\eta} = r\Lambda_0^0(1 - \alpha_0^0)\, e^{\theta_1^0}, \tag{A.2}$$

subject to

$$\alpha_0^0 \to 1, \ \theta_1^0 \to 0 \ \text{as} \ \eta \to +\infty; \quad \alpha_0^0 \to \alpha_s, \ \theta_1^0 \sim E_1^0 \eta \ \text{as} \ \eta \to -\infty, \tag{A.3}$$

where E_1^0 is given by the first of Eqs. (44) with T_b replaced by its leading-order approximation B_1. The first of Eqs. (A.2) is readily integrated from $\alpha_0^0 = \alpha_s$ (at $\eta = -\infty$) to any $\alpha_0^0 \le 1$ (at $\eta = +\infty$) to give

$$e^{\theta_1^0(\alpha_0^0)} = \frac{(b - \hat{b})B_1}{(B_1 - 1)r\Lambda_0^0} \int_{\alpha_s}^{\alpha_0^0} \frac{d\overline{\alpha}}{l + (\hat{l} - l)\overline{\alpha}}. \tag{A.4}$$

Evaluating Eq. (A.4) at $\alpha_0^0 = 1$ (at which $\theta_1^0 = 0$) thus determines the leading-order coefficient Λ_0^0 in the expansion of the burning-rate eigenvalue as

$$\Lambda_0^0 = \begin{cases} \dfrac{(b - \hat{b})B_1 + Q_l}{(B_1 - 1)r(\hat{l} - l)} \ln\left[\dfrac{\hat{l}}{l + (\hat{l} - l)\alpha_s}\right], & l \neq \hat{l} \\ \dfrac{(b - \hat{b})B_1 + Q_l}{(B_1 - 1)rl}(1 - \alpha_s), & l = \hat{l}. \end{cases} \tag{A.5}$$

Substituting this result into Eq. (A.4) for arbitrary α_0 and performing the indicated integration, we thus obtain

$$\theta_1^0(\alpha_0^0) = \begin{cases} \ln\left(\dfrac{\ln\left[l + (\hat{l} - l)\alpha_0^0\right] - \ln\left[l + (\hat{l} - l)\alpha_s\right]}{\ln \hat{l} - \ln\left[l + (\hat{l} - l)\alpha_s\right]}\right), & \hat{l} \neq l \\ \ln\left(\dfrac{\alpha_0^0 - \alpha_s}{1 - \alpha_s}\right), & \hat{l} = l. \end{cases} \tag{A.6}$$

The determination of $\alpha_0^0(\eta)$, and hence $\theta_1^0(\eta)$, then follows directly from the second of Eqs. (A.2). For example, when $\hat{l} = l$ (equal gas and liquid thermal conductivities), we obtain

$$\alpha_0^0(\eta) = \frac{\alpha_s + \exp\left\{l^{-1}\left[(b - \hat{b})B_1 + Q_l\right](1 - \alpha_s)\eta/(B_1 - 1)\right\}}{1 + \exp\left\{l^{-1}\left[(b - \hat{b})B_1 + Q_l\right](1 - \alpha_s)\eta/(B_1 - 1)\right\}}, \tag{A.7}$$

where the matching condition at $\eta = -\infty$ has been used to evaluate the constant of integration.

The first approximation, Eq. (A.5), for the burning-rate eigenvalue is independent of the effects of the second reaction (1b), which has been assumed to have a relatively small thermal effect. Consequently, the first effects of the two-step mechanism on the burning rate appear at $O(\epsilon)$, which requires the calculation of the next-order coefficient Λ_0^1. We thus proceed by first calculating the leading-order mass fraction variable y_1^0, which is determined from the leading-order version of Eq. (46). For additional simplicity, we restrict further consideration to the parameter regime

$$\alpha_s = \alpha_s^1 \epsilon, \quad \hat{l} = l + \epsilon \hat{l}^1, \quad \nu = 1 + \epsilon \nu^1, \tag{A.8}$$

corresponding to $O(\epsilon)$ values of the initial porosity, $O(\epsilon)$ differences in the conductivities of the condensed and gaseous phases, and $O(\epsilon\beta)$ differences in the activation energies of the two reaction steps. In addition, we consider only the case of a first-order gas-phase reaction (*i.e.*, $n = 1$), and assume that

$$\frac{\lambda\overline{\phi}}{rw\Lambda_0^0 T_b^0}\cdot\frac{\hat{b}Le}{rl} = \lambda_0 + \epsilon\lambda_1\,, \tag{A.9}$$

where $T_b^0 = (Q_l+1+\gamma_s)/\hat{b}$ is the leading-order approximation to T_b with respect to ϵ in the above parameter regime. The parameter group on the left-hand side of Eq. (A.9) is a gas-to-liquid ratio of diffusion-weighted reaction rates, where the latter may be interpreted as characteristic measures of the rate of depletion of the reacting species, taking into account both chemical reaction and, for the gas phase, species diffusion. Such quantities appear to arise naturally in the analysis of multi-step flames, and, based on the above interpretation, have been referred to as consumption rates.[14,15] The fact that larger gas-phase Lewis numbers are associated with higher rates of depletion of the gaseous reactant stems from the higher concentration of this species in the reaction zone that results from smaller values of the gas-phase mass diffusivity.

In the parameter regime just outlined, the expressions (A.5) and (A.6) for θ_1^0 and Λ_0^0 simplify to

$$\theta_1^0 = \ln\alpha_0^0\,, \quad \Lambda_0^0 = \frac{bQ_l + (b-\hat{b})(1+\gamma_s)}{rl(Q_l+1+\gamma_s-\hat{b})}\,, \tag{A.10}$$

where, for $\alpha_s \sim O(\epsilon)$, Eq. (A.7) implies

$$\alpha_0^0(\eta) = \frac{\exp\left(r\Lambda_0^0\eta\right)}{1+\exp\left(r\Lambda_0^0\eta\right)}\,, \quad \text{or} \quad \eta = \frac{1}{r\Lambda_0^0}\ln\left(\frac{\alpha_0^0}{1-\alpha_0^0}\right)\,. \tag{A.11}$$

Consequently, the leading-order version of Eq. (46) for y_1^0 as a function of α_0^0 is given by

$$\frac{d^2y_1^0}{d{\alpha_0^0}^2} + \left(\frac{2}{\alpha_0^0} - \frac{1}{1-\alpha_0^0}\right)\frac{dy_1^0}{d\alpha_0^0} - \frac{\lambda_0 y_1^0}{\alpha_0^0(1-\alpha_0^0)^2} = -\frac{\hat{b}\,Le}{rl\Lambda_0^0}\cdot\frac{1}{(\alpha_0^0)^2(1-\alpha_0^0)}\,, \tag{A.12}$$

subject to $y_1^0 \to 0$ as $\alpha_0^0 \to 1$ and an appropriate matching condition as $\alpha_0^0 \to 0$. The latter, however, cannot be obtained directly from Eq. (43) because that equation was derived under the assumption that $\alpha_s \neq 0$, whereas to leading order in ϵ, α_s is equal to zero. Indeed, at this order, the outer solution (33) for Y^0 has no meaning for $\xi < 0$, since there is no gaseous phase in this region at this order of approximation. To derive the appropriate matching conditions on the inner mass fraction variables y_1^0 and, for later use, y_1^1, it is appropriate to consider a new variable Z, defined as the mass fraction of the intermediate gas-phase species with respect to the total mass of all species, gaseous and condensed, at a given point.[10] Thus, Z, which is physically unambiguous in the limit $\alpha \to 0$ (where it must vanish), is defined in terms of the variables already introduced as $Z = \hat{r}\alpha\rho_g Y/[\hat{r}\alpha\rho_g + r(1-\alpha)] = \hat{r}\overline{\phi}\alpha Y/\{\hat{r}\overline{\phi}\alpha + r(1-\alpha)[Y + w(1-Y)]T\}$. From the outer solution written in terms of the inner variable, it is thus seen that the required behavior of Z as $\eta \to -\infty$ is $Z \sim \epsilon\beta^{-1}(\hat{r}\overline{\phi}\alpha_s^1\hat{b}Le/rwT_b^0 l)(-\hat{r}\phi\eta + h_1^0)$. Hence, substituting the inner expansions into the above definition of Z, and imposing this asymptotic behavior, leads to the matching conditions

$$\alpha_0^0 y_1^0 \to 0\,, \;\; \alpha_0^0 y_1^1 \sim -\alpha_s^1 y_1^0 + \alpha_s^1\frac{\hat{b}Le}{l}\left(-\frac{\hat{r}\phi}{r\Lambda_0^0}\ln\alpha_0^0 + h_1^0\right) \;\text{ as }\; \alpha_0^0 \to 0\,, \tag{A.13}$$

where we have used Eq. (A.11) to write these conditions in terms of α_0^0 as α_0^0 tends to zero, and have used the fact that $\alpha_0^1 \to \alpha_s^1$ in this limit.

Solutions to Eq. (A.12) can be expressed formally in terms of hypergeometric functions, but since we desire explicit representations for use in the next-order problem, we focus instead on such solutions that may be obtained for particular values of λ_0. In particular, the solutions for $\lambda_0 = 1$ and $\lambda_0 = 4$ that satisfy the above matching conditions are given by[10,11]

$$y_1^0 = -\frac{\hat{b}\,Le}{2rl\Lambda_0^0} \cdot \begin{cases} 1 + \dfrac{1-\alpha_0^0}{\alpha_0^0} \ln\left(\dfrac{1-\alpha_0^0}{\alpha_0^0}\right) + \dfrac{\ln \alpha_0^0}{\alpha_0^0(1-\alpha_0^0)}\,, & \lambda_0 = 1\,, \\ \dfrac{3-\alpha_0^0}{1-\alpha_0^0} + \dfrac{2\ln \alpha_0^0}{(1-\alpha_0^0)^2}\,, & \lambda_0 = 4\,, \end{cases} \tag{A.14}$$

which completes our analysis of the leading-order reaction-zone problem. We observe that although $\alpha_0^0 y_1^0$ approaches zero in the limit that α_0^0 becomes small, as required by the first of Eqs. (A.13), the variable y_1^0 itself is unbounded in that limit, exhibiting the behavior

$$y_1^0 \sim -(\hat{b}Le/rl\Lambda_0^0) \cdot \begin{cases} \ln \alpha_0^0\,, & \lambda_0 = 1\,, \\ \ln \alpha_0^0 + \dfrac{3}{2}\,, & \lambda_0 = 4\,, \end{cases} \tag{A.15}$$

as $\alpha_0^0 \to 0$.

The reaction-zone problem at the next order (with respect to ϵ) is obtained by collecting terms of order ϵ when the expansions (A.1), (A.8) and (A.9) are substituted into Eqs. (39) - (43). This results in a problem for the next-order quantities α_0^1, y_1^1 and θ_1^1 and Λ_0^1, as well as the leading-order coefficient h_1^0, which is still to be determined. As before, the equations for α_0^1 and θ_1^1 decouple from the equation for y_1^1. These are given by

$$\frac{d\alpha_0^1}{d\eta} = r\left[\Lambda_0^0(1-\alpha_0^0)\theta_1^1 + \Lambda_0^1(1-\alpha_0^0) - \Lambda_0^0\alpha_0^1\right] e^{\theta_1^0}\,, \tag{A.16}$$

$$l\frac{d\theta_1^1}{d\eta} + \hat{l}^1\alpha_0^0\frac{d\theta_1^0}{d\eta} + \frac{lQ_g^1}{\hat{b}Le(T_b^0-1)}\alpha_0^0\frac{dy_1^0}{d\eta} = -C_0\alpha_0^1 + C_1(1-\alpha_0^0)\,, \tag{A.17}$$

subject to the matching conditions

$$\alpha_0^1 \to 0\,,\ \ \theta_1^1 \to 0 \ \text{ as } \ \eta \to +\infty\,; \quad \alpha_0^1 \to \alpha_s^1\,,\ \ \theta_1^1 \sim E_1^1\eta + E_2^1 h_1^0 \ \text{ as } \ \eta \to -\infty\,, \tag{A.18}$$

where, from the last of Eqs. (34) and (35) and the first of Eqs. (A.8), the coefficients C_0, C_1 and E_1^1 are given by

$$C_0 = \frac{(b-\hat{b})T_b^0 + Q_l}{T_b^0 - 1} = rl\Lambda_0^0\,, \quad C_1 = \frac{Q_g^1(T_b^0-1) - T_b^1(Q_l + b - \hat{b})}{(T_b^0-1)^2}\,, \tag{A.19}$$

$$E_1^1 = \frac{\alpha_s^1(\hat{r}\hat{b} - b)}{l} + \frac{[\alpha_s^1(T_b^0-1) + T_b^1](1+\gamma_s - b)}{l(T_b^0-1)^2}\,, \quad E_2^1 = -\frac{Q_g^1}{l(T_b^0-1)}\,, \tag{A.20}$$

and where

$$T_b \sim T_b^0 + \epsilon T_b^1 + \cdots\,, \quad T_b^0 = \frac{Q_l + 1 + \gamma_s}{\hat{b}}\,, \quad T_b^1 = \frac{Q_g^1}{\hat{b}} - \hat{r}(T_b^0 - 1)\alpha_s^1\,. \tag{A.21}$$

We observe that T_b^1, and hence C_1 and E_1^1, all depend on α_s^1, reflecting, to this order of approximation, a linearly decreasing dependence of the burned temperature on the initial porosity for small values of the latter.

It is again convenient to use the volume-fraction variable α_0^0 as the independent variable, which transforms Eqs. (A.16) and (A.17) into a somewhat simpler form. In particular, using the transformation rule $d/d\eta = r\Lambda_0^0\alpha_0^0(1-\alpha_0^0)d/d\alpha_0^0$ according to Eq. (39), we obtain

$$\frac{d\alpha_0^1}{d\alpha_0^0} + \frac{\alpha_0^1}{1-\alpha_0^0} = \theta_1^1 + \frac{\Lambda_0^1}{\Lambda_0^0}, \tag{A.22}$$

$$rl\Lambda_0^0\alpha_0^0(1-\alpha_0^0)\frac{d\theta_1^1}{d\alpha_0^0} + C_0\alpha_0^1 = C_1(1-\alpha_0^0) - r\hat{l}^1\Lambda_0^0\alpha_0^0(1-\alpha_0^0) - \frac{Q_g^1 rl\Lambda_0^0}{\hat{b}\,Le(T_b^0-1)}(\alpha_0^0)^2(1-\alpha_0^0)\frac{dy_1^0}{d\alpha_0^0}, \tag{A.23}$$

subject to the matching conditions (A.18). Upon substitution of the expressions for y_1^0 given by Eq. (A.14), this subproblem may be solved for α_0^1 and θ_1^1 as follows. First, we rewrite Eq. (A.22) as $(d/d\alpha_0^0)[\alpha_0^1/(1-\alpha_0^0)] = (\theta_1^1 + \Lambda_0^1/\Lambda_0^0)/(1-\alpha_0^0)$. Then, dividing Eq. (A.23) by $1-\alpha_0^0$ and differentiating with respect to α_0^0, a single second-order equation for θ_1^1 is obtained as

$$\frac{d^2\theta_1^1}{d{\alpha_0^0}^2} + \frac{1}{\alpha_0^0}\frac{d\theta_1^1}{d\alpha_0^0} + \frac{\theta_1^1}{\alpha_0^0(1-\alpha_0^0)} = -\frac{Q_g^1}{\hat{b}\,Le(T_b^0-1)}\frac{1}{\alpha_0^0}\frac{d}{d\alpha_0^0}\left[(\alpha_0^0)^2\frac{dy_1^0}{d\alpha_0^0}\right] - \frac{\Lambda_0^1/\Lambda_0^0}{\alpha_0^0(1-\alpha_0^0)} - \frac{\hat{l}^1/l}{\alpha_0^0}, \tag{A.24}$$

where we have used the fact that $C_0 = rl\Lambda_0^0$.

Homogeneous solutions of Eq. (A.24) are $1-\alpha_0^0$ and $(1-\alpha_0^0)\ln\left[\alpha_0^0(1-\alpha_0^0)^{-1}\right]+1$, and thus construction of the general solution for θ_1^1 may be achieved by reduction of order, and substituted into the first-order Eq. (A.22) to determine α_0^1. In this way, we obtain, for example, the general solution corresponding to $\lambda_0 = 4$ as

$$\begin{aligned}\theta_1^1 = {} & c_1\left[1 + (1-\alpha_0^0)\ln\left(\frac{\alpha_0^0}{1-\alpha_0^0}\right)\right] + c_2(1-\alpha_0^0) - \frac{\Lambda_0^1}{\Lambda_0^0} + \frac{\hat{l}^1}{2l}(1-\alpha_0^0)\ln\alpha_0^0 \\ & + \frac{Q_g^1}{rl\Lambda_0^0(T_b^0-1)}\left\{\frac{1}{1-\alpha_0^0} + \frac{9}{2} + \frac{\ln\alpha_0^0}{(1-\alpha_0^0)^2} - \frac{5\ln\alpha_0^0}{2(1-\alpha_0^0)} - 2\ln\alpha_0^0 + \frac{13}{2}(1-\alpha_0^0)\ln\left(\frac{\alpha_0^0}{1-\alpha_0^0}\right)\right. \\ & \left. + 2(1-\alpha_0^0)\left[\frac{\pi^2}{6} + \mathrm{Li}_2(\alpha_0^0)\right]\ln\alpha_0^0 + 2\mathrm{Li}_2(1-\alpha_0^0) - 2(1-\alpha_0^0)\left[2\mathrm{Li}_3(\alpha_0^0) + \mathrm{Li}_3(1-\alpha_0^0)\right]\right\},\end{aligned} \tag{A.25}$$

$$\begin{aligned}\alpha_0^1 = {} & c_3(1-\alpha_0^0) + (1-\alpha_0^0)\left[c_1\alpha_0^0\ln\left(\frac{\alpha_0^0}{1-\alpha_0^0}\right) + c_2\alpha_0^0 + \frac{\hat{l}^1}{2l}\left(\alpha_0^0\ln\alpha_0^0 - \alpha_0^0\right)\right] \\ & + \frac{Q_g^1(1-\alpha_0^0)}{rl\Lambda_0^0(T_b^0-1)}\left\{\frac{1}{2(1-\alpha_0^0)}\left(1 + \frac{\ln\alpha_0^0}{1-\alpha_0^0}\right) - \left[\frac{1+4\alpha_0^0}{2(1-\alpha_0^0)} - \left(\frac{\pi^2}{3} + \frac{13}{2}\right)\alpha_0^0\right]\ln\alpha_0^0\right. \\ & \left. - \frac{13}{2}\alpha_0^0\ln(1-\alpha_0^0) + 2\alpha_0^0\mathrm{Li}_2(\alpha_0^0)\ln\alpha_0^0 - 2\mathrm{Li}_2(1-\alpha_0^0) - 4\alpha_0^0\mathrm{Li}_3(\alpha_0^0) - 2\alpha_0^0\mathrm{Li}_3(1-\alpha_0^0)\right\},\end{aligned} \tag{A.26}$$

where c_1, c_2 and c_3 are constants of integration, and where we have introduced the polylogarithm functions $\mathrm{Li}_n(\alpha)$, $n \geq 2$.[21] These are defined recursively for all complex α by

$$\mathrm{Li}_2(\alpha) = -\int_0^\alpha \frac{\ln(1-\overline{\alpha})}{\overline{\alpha}}\,d\overline{\alpha} = \sum_{j=1}^\infty \frac{\alpha^j}{j^2}, \quad \mathrm{Li}_{n>2}(\alpha) = \int_0^\alpha \frac{\mathrm{Li}_{n-1}(\overline{\alpha})}{\overline{\alpha}}\,d\overline{\alpha} = \sum_{j=1}^\infty \frac{\alpha^j}{j^n}, \tag{A.27}$$

where the latter form of the representation is convergent for $|\alpha| \leq 1$. In the real domain of interest here $(0 \leq \alpha \leq 1)$, $\mathrm{Li}_2(\alpha)$ and $\mathrm{Li}_3(\alpha)$ are monotonic functions that range from $\mathrm{Li}_2(0) = \mathrm{Li}_3(0) = 0$ to $\mathrm{Li}_2(1) = \pi^2/6$ and $\mathrm{Li}_3(1) \doteq 1.20205690$, respectively. We also note the identity $\mathrm{Li}_2(\alpha) + \mathrm{Li}_2(1-\alpha) = \pi^2/6 - \ln\alpha\,\ln(1-\alpha)$, which was used in obtaining Eqs. (A.25) and (A.26). Application of the matching conditions (A.8) then determines Λ_1^1, c_1, c_2 and c_3 as

$$\Lambda_0^1 = \frac{Q_g^1}{rl(T_b^0-1)}\left(\frac{7}{2} - \frac{\pi^2}{3}\right) + \frac{1}{r}E_1^1 - \frac{\hat{l}^1}{2l}\Lambda_0^0, \tag{A.28}$$

$$c_1 = -\frac{Q_g^1}{rl\Lambda_0^0(T_b^0-1)}\left(3+\frac{\pi^2}{3}\right)+\frac{E_1^1}{r\Lambda_0^0}-\frac{\hat{l}^1}{2l}, \tag{A.29}$$

$$c_2 = \frac{Q_g^1}{rl\Lambda_0^0(T_b^0-1)}\left[1-\frac{\pi^2}{3}+2\mathrm{Li}_3(1)\right]-\frac{Q_g^1}{l(T_b^0-1)}h_1^0, \tag{A.30}$$

$$c_3 = \alpha_s^1+\frac{Q_g^1}{rl\Lambda_0^0(T_b^0-1)}\left(\frac{\pi^2}{3}-\frac{1}{2}\right), \tag{A.31}$$

where E_1^1 was defined by Eq. (A.20), and we note that c_2 is given in terms of h_1^0.

An expression for h_1^0 may be determined by continuing with the analysis,[10] but its value can be deduced directly from the second of the matching conditions (A.13) as follows. Substituting the second line of Eq. (A.15) into Eq. (A.13) leads to the condition that

$$y_1^1 \sim \alpha_s^1\frac{\hat{b}Le}{rl\Lambda_0^0}\cdot\frac{1}{\alpha_0^0}\left[(1-\hat{r}\phi)\ln\alpha_0^0+r\Lambda_0^0h_1^0+\frac{3}{2}\right], \quad \lambda_0=4, \tag{A.31}$$

as $\alpha_0^0 \to 0$. Since $1/\alpha_0^0 \sim \exp(-r\Lambda_0^0\eta)$ as the inner variable $\eta \to -\infty$, Eq. (A.31) implies that y_1^1 grows exponentially as $\eta \to -\infty$ unless the right-hand side of Eq. (A.13) is identically zero. Since only algebraic growth of the inner solution is compatible with an asymptotic matching with the outer solution, as indicated in Eq. (43), we conclude from Eq. (A.13) that $\hat{r}\phi = 1+\mathrm{O}(\epsilon)$ and that $h_1^0 = (-3/2)/(r\Lambda_0^0)$. This required restriction of $\hat{r}$ to values that are relatively close to $1/\phi \geq 1$ corresponds to the assumption of high upstream gas-phase densities, or pressures, and may be interpreted as a compatibility condition, required for the existence of a merged-flame solution, that accompanies our ordering of the activation energies and consumption rates when gas-phase heat release is small. According to the expression (26) for the gas-phase velocity, it essentially limits the two-phase-flow effect (the rate of gas-phase convective transport relative to the condensed phase) to that associated with thermal expansion of the gas. Larger rates of gas-phase transport with respect to that in the condensed phase would cause the gas-phase reaction to occur increasingly downstream of the condensed reaction, leading to a breakdown in the merged flame structure analyzed here, but the numerical results presented in the main body of the paper suggest, since h_1 is a decreasing function of λ, that larger gas-phase consumption rates allow for larger gas-phase convective transport arising from smaller upstream gas densities. A similar calculation can be performed for $\lambda_0 = 1$, which leads to $h_1^0 = 0$ and an expression for Λ_0^1 identical to Eq. (A.28) except for the factor $7/2-\pi^2/3$, which is replaced by the factor $\pi^2/6-1$.[10] Profiles of the two-term perturbation solution (one term in the case of y_1 and h_1) are exhibited in Figure 2 for $\lambda_0 = 1$, in which case the second-order terms θ_1^1 and α_0^1 are given by

$$\begin{aligned}\theta_1^1 = {} & c_1\left[1+(1-\alpha_0^0)\ln\left(\frac{\alpha_0^0}{1-\alpha_0^0}\right)\right]+c_2(1-\alpha_0^0)-\frac{\Lambda_0^1}{\Lambda_0^0}+\frac{\hat{l}^1}{2l}(1-\alpha_0^0)\ln\alpha_0^0 \\ & +\frac{Q_g^1}{2rl\Lambda_0^0(T_b^0-1)}\left\{\frac{\ln\alpha_0^0}{1-\alpha_0^0}-(1-\alpha_0^0)\ln\left(\frac{\alpha_0^0}{1-\alpha_0^0}\right)-1-\left[\frac{\pi^2}{3}+2\mathrm{Li}_2(\alpha_0^0)\right](1-\alpha_0^0)\ln\alpha_0^0\right. \\ & \left.+2\alpha_0\ln\alpha_0^0+2(1-\alpha_0^0)\left[2\mathrm{Li}_3(\alpha_0^0)+\mathrm{Li}_3(1-\alpha_0^0)\right]-2\left[\mathrm{Li}_2(1-\alpha_0^0)+(1-\alpha_0^0)\ln(1-\alpha_0^0)\right]\right\},\end{aligned} \tag{A.32}$$

$$\begin{aligned}\alpha_0^1 = {} & c_3(1-\alpha_0^0)+(1-\alpha_0^0)\left[c_1\alpha_0^0\ln\left(\frac{\alpha_0^0}{1-\alpha_0^0}\right)+c_2\alpha_0^0+\frac{\hat{l}^1}{2l}\left(\alpha_0^0\ln\alpha_0^0-\alpha_0^0\right)\right] \\ & +\frac{Q_g^1(1-\alpha_0^0)}{rl\Lambda_0^0(T_b^0-1)}\left\{\left[\frac{3\alpha_0^0-2}{2(1-\alpha_0^0)}-\frac{\pi^2}{6}\right]\alpha_0^0\ln\alpha_0^0+\frac{1}{2}(3\alpha_0^0-1)\ln(1-\alpha_0^0)\right. \\ & \left.-\alpha_0^0\ln\alpha_0^0\,\mathrm{Li}_2(\alpha_0^0)+\mathrm{Li}_2(1-\alpha_0^0)+2\alpha_0^0\mathrm{Li}_3(\alpha_0^0)+\alpha_0^0\mathrm{Li}_3(1-\alpha_0^0)\right\},\end{aligned} \tag{A.33}$$

where

$$c_1 = \frac{Q_g^1 \pi^2}{6rl\Lambda_0^0(T_b^0-1)} + \frac{E_1^1}{r\Lambda_0^0} - \frac{\hat{l}^1}{2l}, \quad c_2 = \frac{Q_g^1}{rl\Lambda_0^0(T_b^0-1)}\left[\frac{\pi^2}{6} - \frac{1}{2} - \mathrm{Li}_3(1) - r\Lambda_0^0 h_1^0\right], \tag{A.34}$$

$$c_3 = \alpha_s^1 - \frac{Q_g^1 \pi^2}{6rl\Lambda_0^0(T_b^0-1)}, \quad \Lambda_0^1 = \frac{Q_g^1}{rl(T_b^0-1)}\left(\frac{\pi^2}{6} - 1\right) + \frac{1}{r}E_1^1 - \frac{\hat{l}^1}{2l}\Lambda_0^0. \tag{A.35}$$

Acknowledgement

This work was supported by the U. S. Department of Energy under Contract DE-AC04-94AL85000. The authors wish to thank Prof. Forman A. Williams of UCSD for fruitful discussions and comments, and Prof. J. R. Cash of Imperial College (London) for helpful suggestions regarding numerical methods for two-point boundary-value problems.

References

1. Baer, M. R., and Nunziato, J. W., "A Two-Phase Mixture Theory for the Deflagration-to-Detonation Transition (DDT) in Reactive Granular Materials," *Int. J. Multiphase Flow*, Vol. 12, 1986, pp. 861–889.
2. Maksimov, E. I., and Merzhanov, A. G., "Theory of Combustion of Condensed Substances," *Combustion, Explosion, and Shock Waves*, Vol. 2, 1966, pp. 25–31.
3. Merzhanov, A. G., "The Theory of Stable Homogeneous Combustion of Condensed Substances," *Combust. Flame*, Vol. 13, 1969, pp. 143–156.
4. Margolis, S. B., Williams, F. A., and Armstrong, R. C., "Influences of Two-Phase Flow in the Deflagration of Homogeneous Solids," *Combust. Flame*, Vol. 67, 1987, pp. 249–258.
5. Li, S. C., Williams, F. A., and Margolis, S. B., "Effects of Two-Phase Flow in a Model for Nitramine Deflagration," *Combust. Flame*, Vol. 80, 1990, pp. 329–349.
6. Margolis, S. B., and Williams, F. A., "Stability of Homogeneous-Solid Deflagration with Two-Phase Flow in the Reaction Zone," *Combust. Flame*, Vol. 79, 1990, pp. 199–213.
7. Margolis, S. B., and Williams, F. A., "Effects of Two-Phase Flow on the Deflagration of Porous Energetic Materials," *J. Propulsion Power*, Vol. 11, 1995, pp. 759–768.
8. Margolis, S. B., and Williams, F. A., "Influence of porosity and two-phase flow on diffusional/thermal instability of a deflagrating energetic material," *Combust. Sci. Technol.*, Vol. 106, 1995, pp. 41–68.
9. Margolis, S. B., and Williams, F. A., "Effect of gas-phase thermal expansion on stability of deflagrations in porous energetic materials. *Int. J. Multiphase Flow*, Vol. 22, 1996, pp. 69–91.
10. Margolis, S. B., "A Deflagration Analysis of Porous Energetic Materials with Two-Phase Flow and a Multiphase Sequential Reaction Mechanism," *Int. J. Eng. Math.*, 1996, submitted.
11. Margolis, S. B., Williams, F. A., and Telengator, A. M., "Combustion of Porous Energetic Materials in the Merged-Flame Regime," *Twenty-Sixth Symposium (International) on Combustion*, 1996, to appear.
12. Prasad, K., Yetter, R. A., and Smooke, M. D., "An Eigenvalue Method for Computing the Burning Rates of RDX Propellants," AIAA Paper #96-0880, 1996.

13. Li, S. C., and Williams, F. A., 'Nitramine Deflagration: Reduced Chemical Mechanism for Primary Flame Facilitating Simplified Asymptotic Analysis," *J. Propulsion and Power*, Vol. 12, 1996, pp. 302–309.

14. Margolis, S. B., and Matkowsky, B. J., "Flame Propagation with a Sequential Reaction Mechanism," *SIAM J. Appl. Math.*, Vol. 42, 1982, pp. 1175–1188.

15. Margolis, S. B., and Matkowsky, B. J., "Steady and Pulsating Modes of Sequential Flame Propagation," *Combust. Sci. Technol.*, Vol. 27, 1982, pp. 193–213.

16. Ascher, U., Mattheij, R. M. M., and Russell, R. D., *Numerical Solution of Boundary Value Problems for Ordinary Differential Equations*, Prentice-Hall, Englewood Cliffs, N. J., 1988.

17. Cash, J. R., "On the Numerical Integration of Nonlinear Two-Point Boundary Value Problems Using Iterated Deferred Corrections, Part 1: A Survey and Comparison of Some One-Step Formulae," *Comput. Math. Appl.*, Vol. 12a, 1986, pp. 1029–1048.

18. Cash, J. R., "On the Numerical Integration of Nonlinear Two-Point Boundary Value Problems Using Iterated Deferred Corrections, Part 2: The Development and Analysis of Highly Stable Deferred Correction Formulae," *SIAM J. Numer. Anal.*, Vol. 25, 1988 pp. 862–882.

19. Cash, J. R., and Wright, M. H., "Implementation Issues in Solving Nonlinear Equations for Two-Point Boundary Value Problems," *Computing*, vol. 45, 1990, pp. 17–37.

20. Cash, J. R., and Wright, M. H., "A Deferred Correction Method for Nonlinear Two-Point Boundary Value Problems: Implementation and Numerical Evaluation," *SIAM J. Sci. Stat. Comput.*, vol. 12, 1991, pp. 971–989.

21. Lewin, L., *Polylogarithms and Associated Functions*, Elsevier North Holland, New York, 1981.

FIGURE CAPTIONS

Figure 1. Outer structure of a leftward-propagating deflagration wave. The solid/gas region lies to the left of $\xi = 0$, and the liquid/gas region to the right. The shaded area denotes the region $\xi_r < \xi < \xi_r + H$, which, despite the explicit representation afforded by the outer delta-function formulation, actually lies within the inner reaction zone. The region to the right of the reaction zone consists of purely gaseous products. Parameter values used were $b = r = Le = l = \phi = 1$, $\hat{b} = \hat{r} = \hat{l} = .8$, $\alpha_s = .25$, $Q_l = 5$, $Q_g = H = .5$, $\gamma_s = -.2$, $T_m = 2$.

Figure 2. Comparison of the asymptotic numerical and analytical solutions for the inner structure and eigenvalues of a leftward-propagating deflagration wave for parameter values consistent with the latter, as described in the Appendix.

Figures 3–11. Plots of (a) the eigenvalues h_1 and Λ_0 as a function of α_s for several different values of one additional parameter, where the arrows denote the appropriate vertical axis for each family of curves. Base values for the parameters were taken to be $r = .75$, $l = b = \hat{l} = \hat{b} = \lambda = Le = \phi = \nu = n = 1$, $\hat{r} = .6$, $w = \tilde{w}_I/\tilde{w}_P = 1.157$, $Q_g = 1.159$, $Q_l = 3.413$, $\gamma_s = .7429$ and $N_l = 64.59/T_b$. Also shown are (b) corresponding plots of $\tilde{U} = (\tilde{\lambda}_s \tilde{A}_l/\tilde{\rho}_s \tilde{c}_s \beta \Lambda_0)^{1/2}\, e^{-N_l/2}$ and $\tilde{H} = (\tilde{\lambda}_s/\tilde{\rho}_s \tilde{c}_s \tilde{U}) h_1/\beta$ as a function of α_s, where $\tilde{H}$ and $\tilde{U}$ are the nonscaled dimensional separation constant and propagation speed, respectively. Dimensional values used to evaluate N_l and $\beta = (1 - T_b^{-1}) N_l$ include $\tilde{T}_u = 360°\mathrm{K}$ and $\tilde{E}_l = 46.0\,\mathrm{kcal/mole}$, and other dimensional values used in the evaluation of $\tilde{U}$ and $\tilde{H}$ include $\tilde{\lambda}_s = 5 \times 10^{-4}\,\mathrm{cal/°K/cm/sec}$, $\tilde{\rho}_s = 1.9\,\mathrm{g/cm^3}$, $\tilde{c}_s = 0.35\,\mathrm{cal/g°K}$, and $\tilde{A}_l = 1 \times 10^{11}/\mathrm{sec}$, where the above solid properties were kept fixed as the gas-to-solid ratios ratios $\hat{\lambda}$, $\hat{r}$ and $\hat{b}$ were varied.

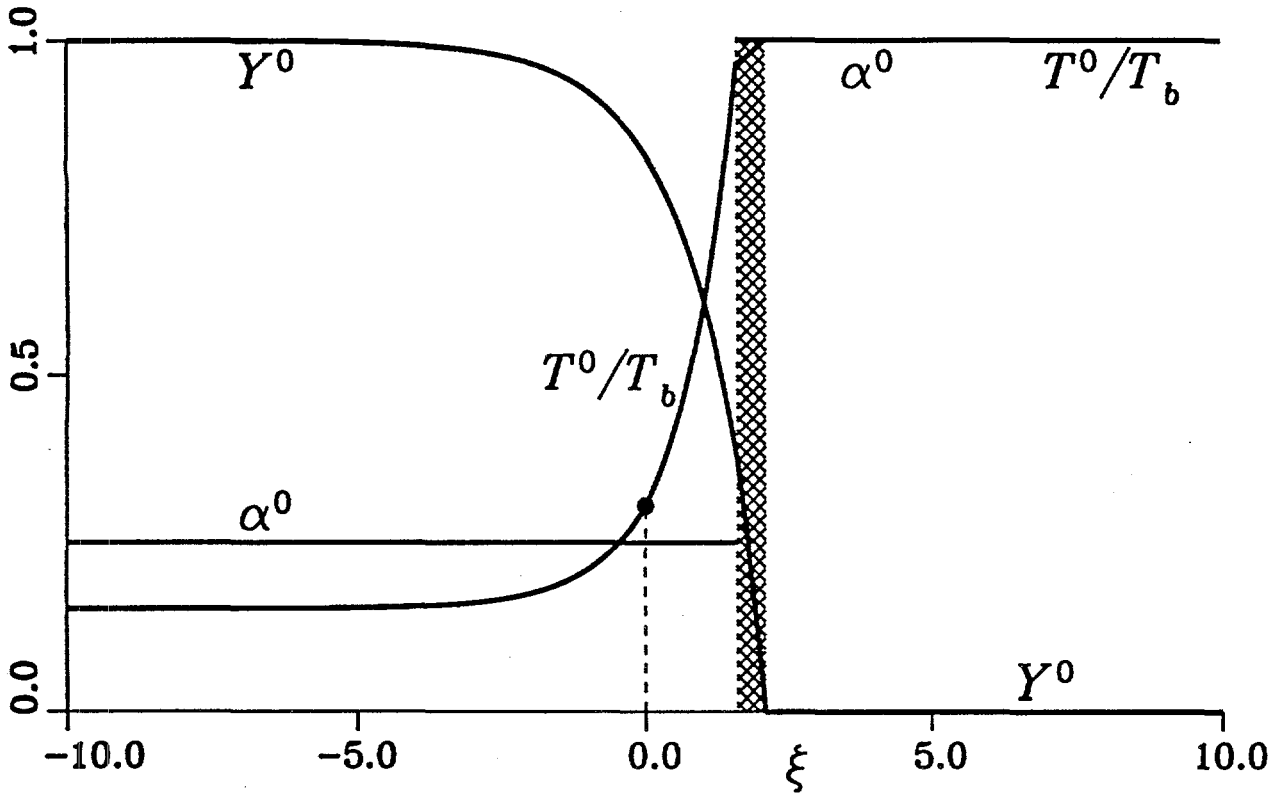

Figure 1

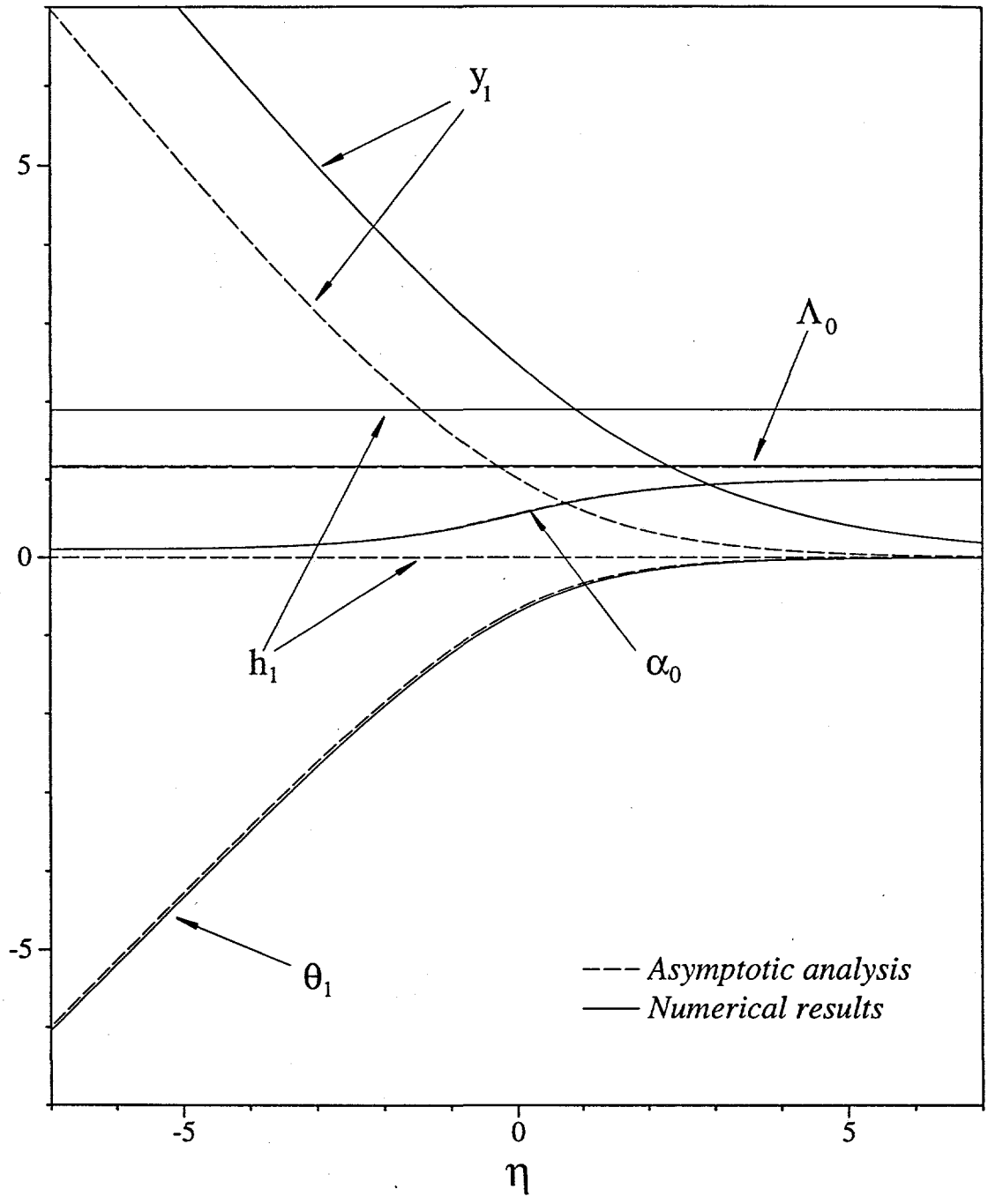
y1
5
Λ0
0
h1
α0
-5
θ1
Asymptotic analysis
Numerical results
-5
0
5
η

Figure 2

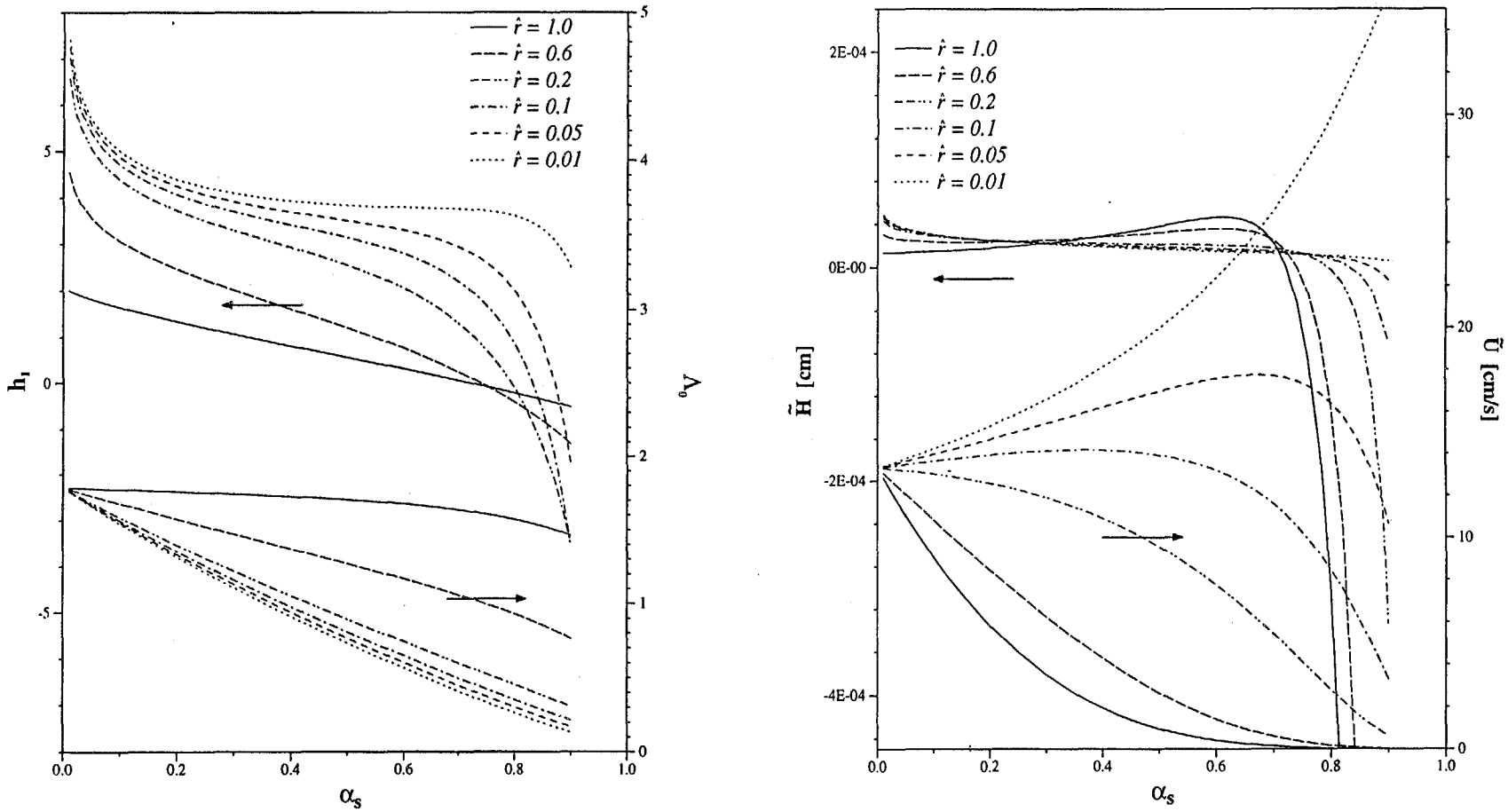
$\hat{r}$ = 1.0
$\hat{r}$ = 0.6
$\hat{r}$ = 0.2
$\hat{r}$ = 0.1
$\hat{r}$ = 0.05
$\hat{r}$ = 0.01
h_1
^0V
α_s
$\tilde{H}$ [cm]
$\tilde{U}$ [cm/s]
2E-04
0E-00
-2E-04
-4E-04

Figure 3a,b

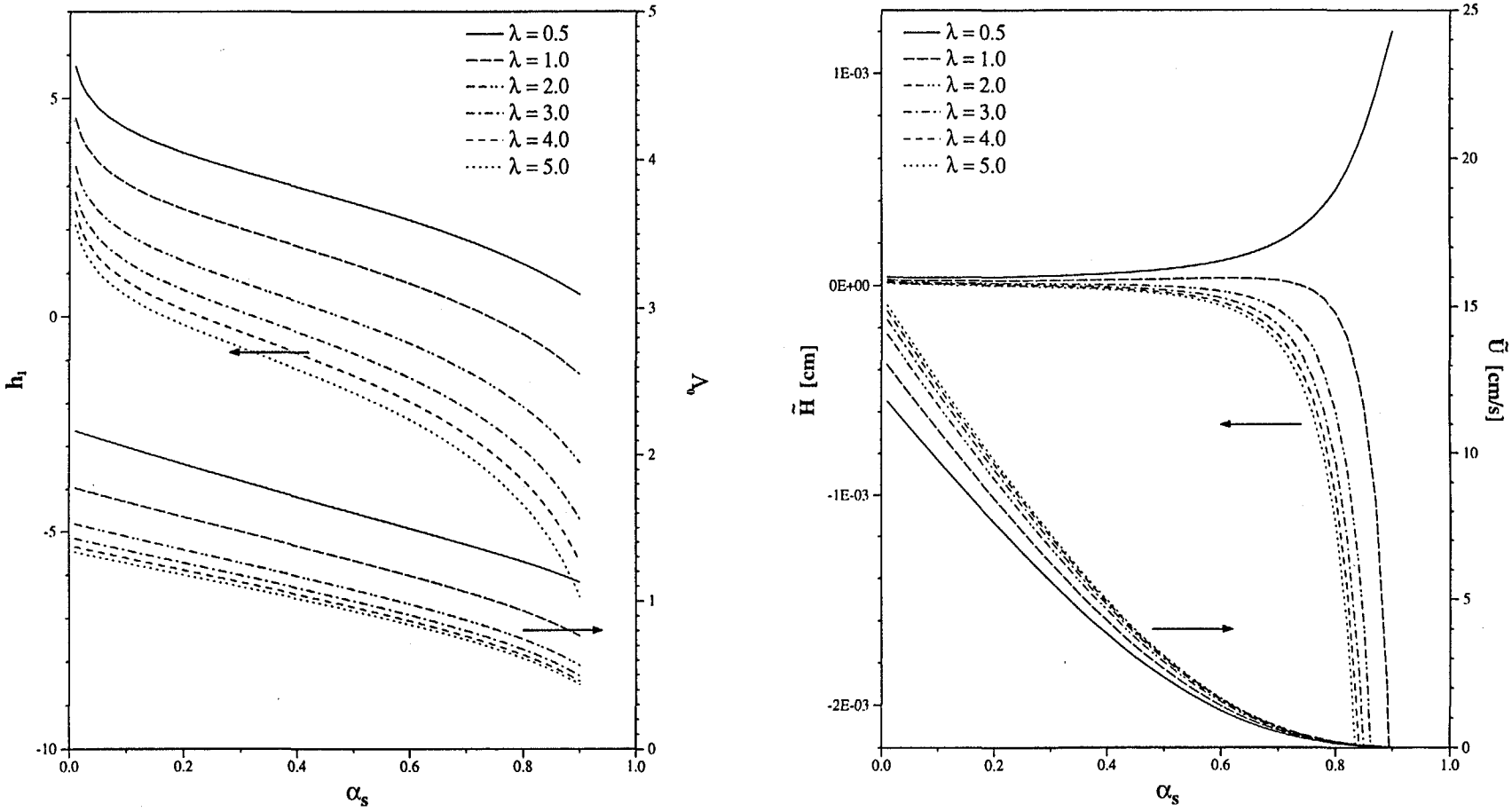
λ = 0.5
λ = 1.0
λ = 2.0
λ = 3.0
λ = 4.0
λ = 5.0
h1
Λ
αs
H̃ [cm]
Ũ [cm/s]
1E-03
0E+00
-1E-03
-2E-03
0.0
0.2
0.4
0.6
0.8
1.0

Figure 4a,b

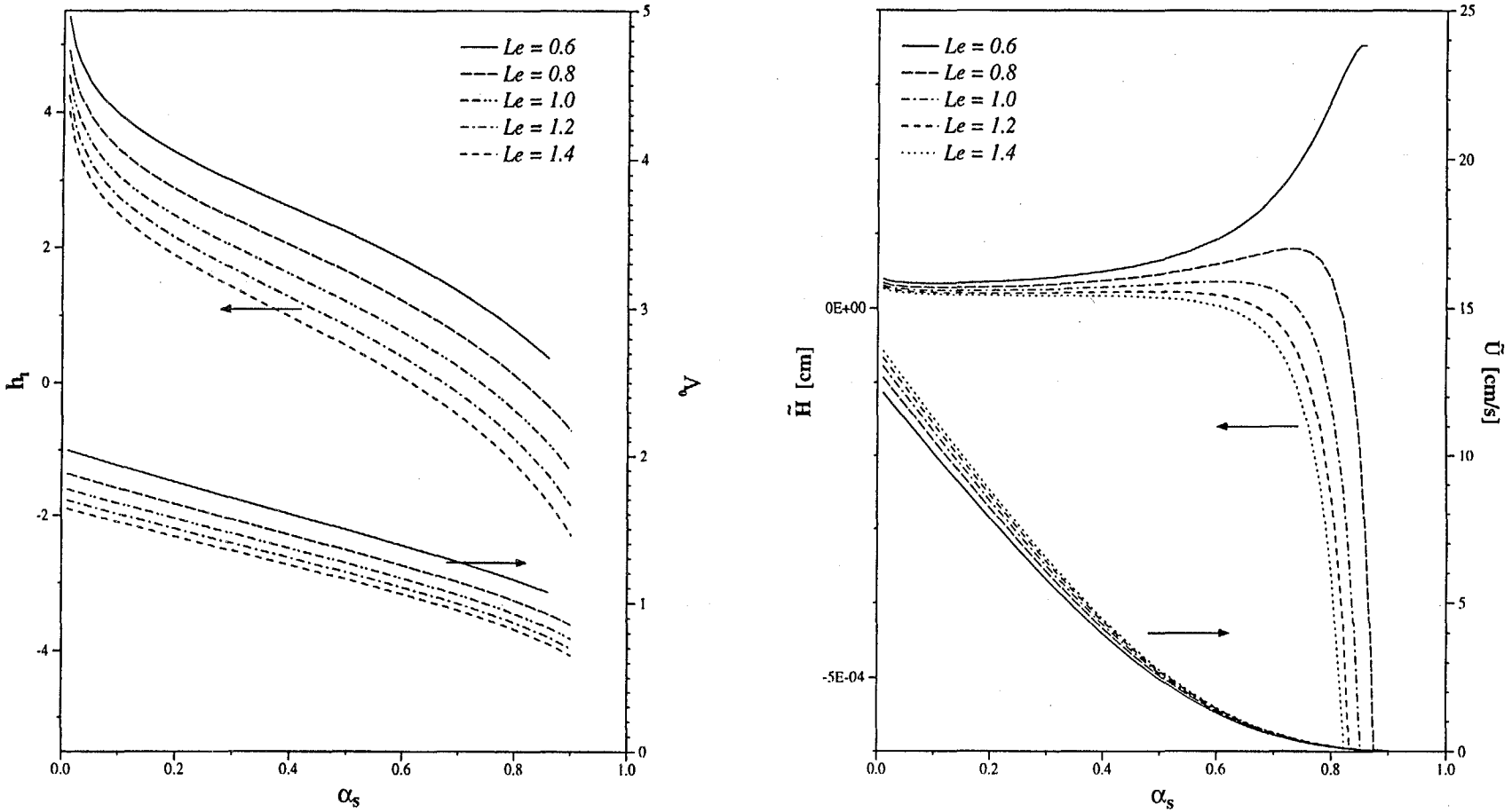

Figure 5a,b

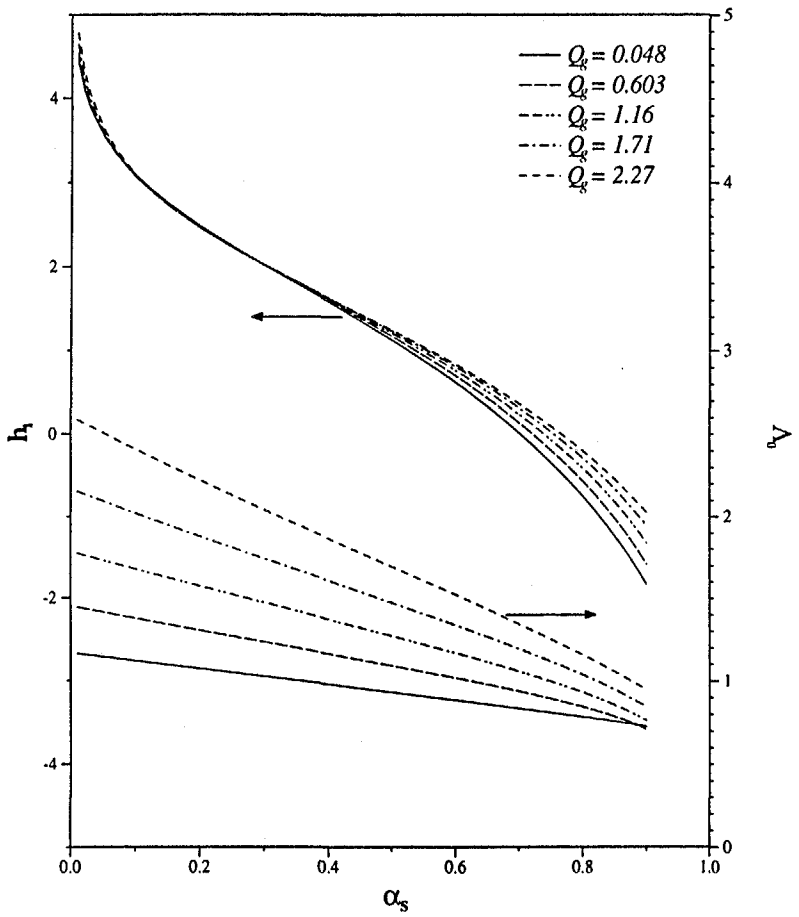
Q_g = 0.048
Q_g = 0.603
Q_g = 1.16
Q_g = 1.71
Q_g = 2.27
h_l
V_g
α_s

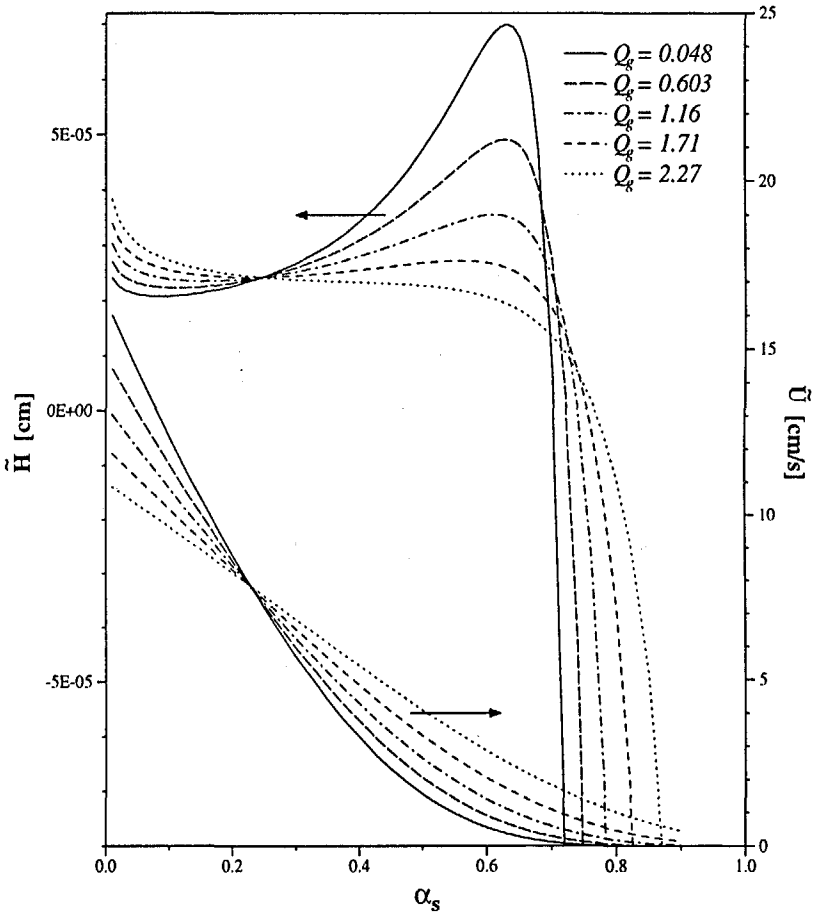
Q_g = 0.048
Q_g = 0.603
Q_g = 1.16
Q_g = 1.71
Q_g = 2.27
$\tilde{H}$ [cm]
$\tilde{U}$ [cm/s]
α_s

Figure 6a,b

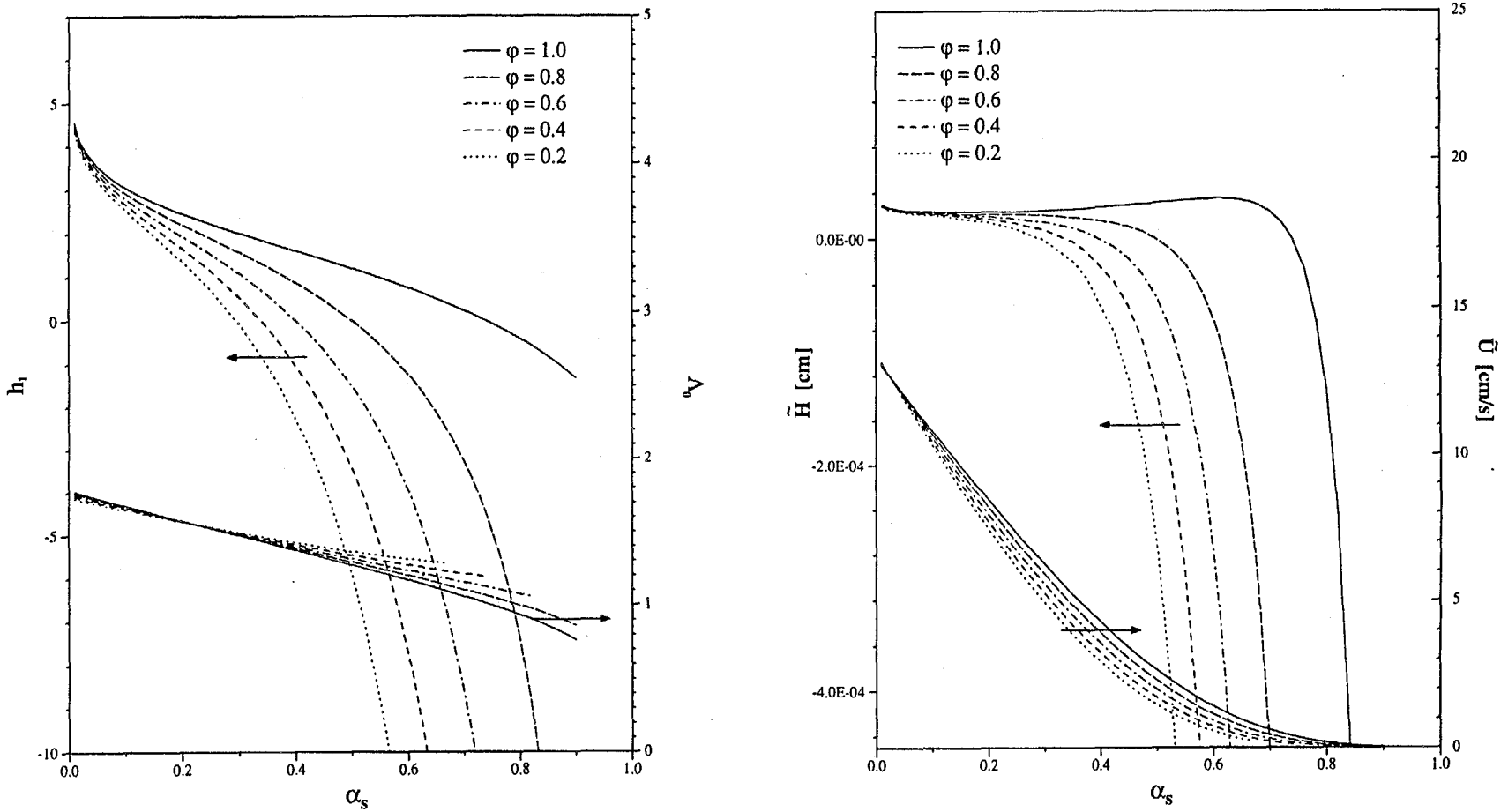

Figure 7a,b

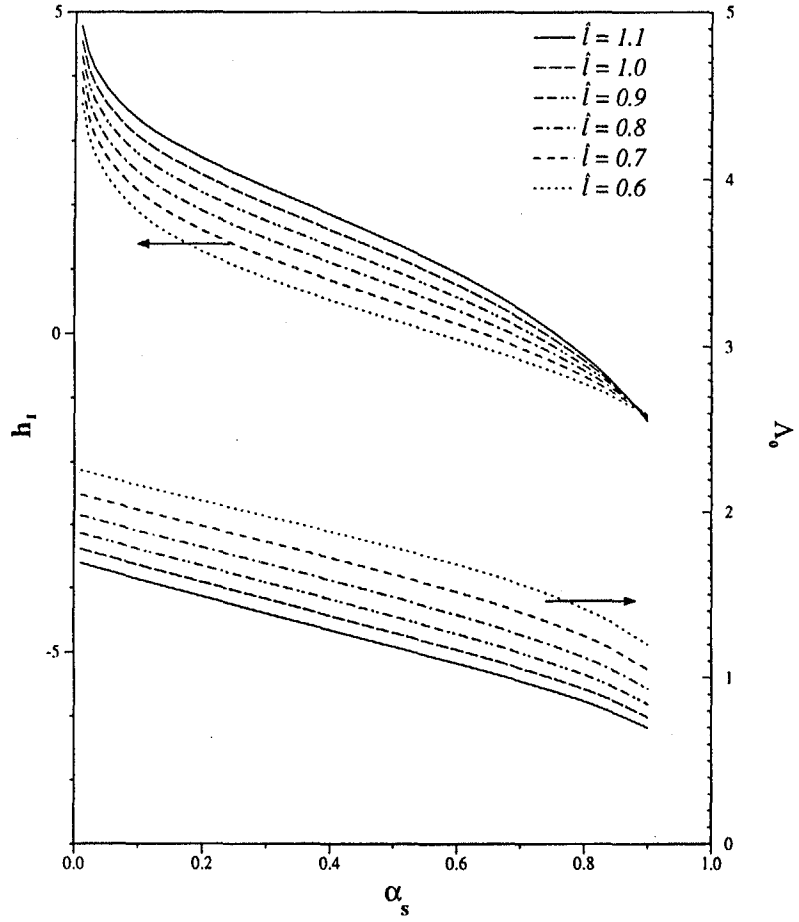
$\hat{l}$ = 1.1
$\hat{l}$ = 1.0
$\hat{l}$ = 0.9
$\hat{l}$ = 0.8
$\hat{l}$ = 0.7
$\hat{l}$ = 0.6
h_1
^oV
α_s

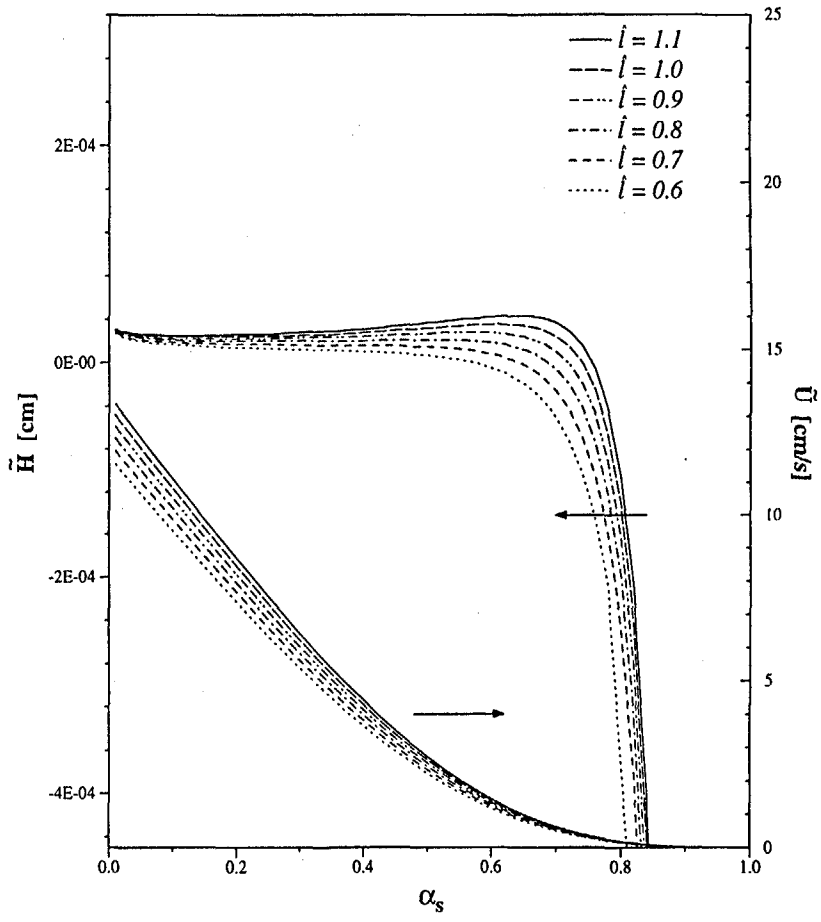
$\hat{l}$ = 1.1
$\hat{l}$ = 1.0
$\hat{l}$ = 0.9
$\hat{l}$ = 0.8
$\hat{l}$ = 0.7
$\hat{l}$ = 0.6
$\tilde{H}$ [cm]
$\tilde{U}$ [cm/s]
α_s

Figure 8a,b

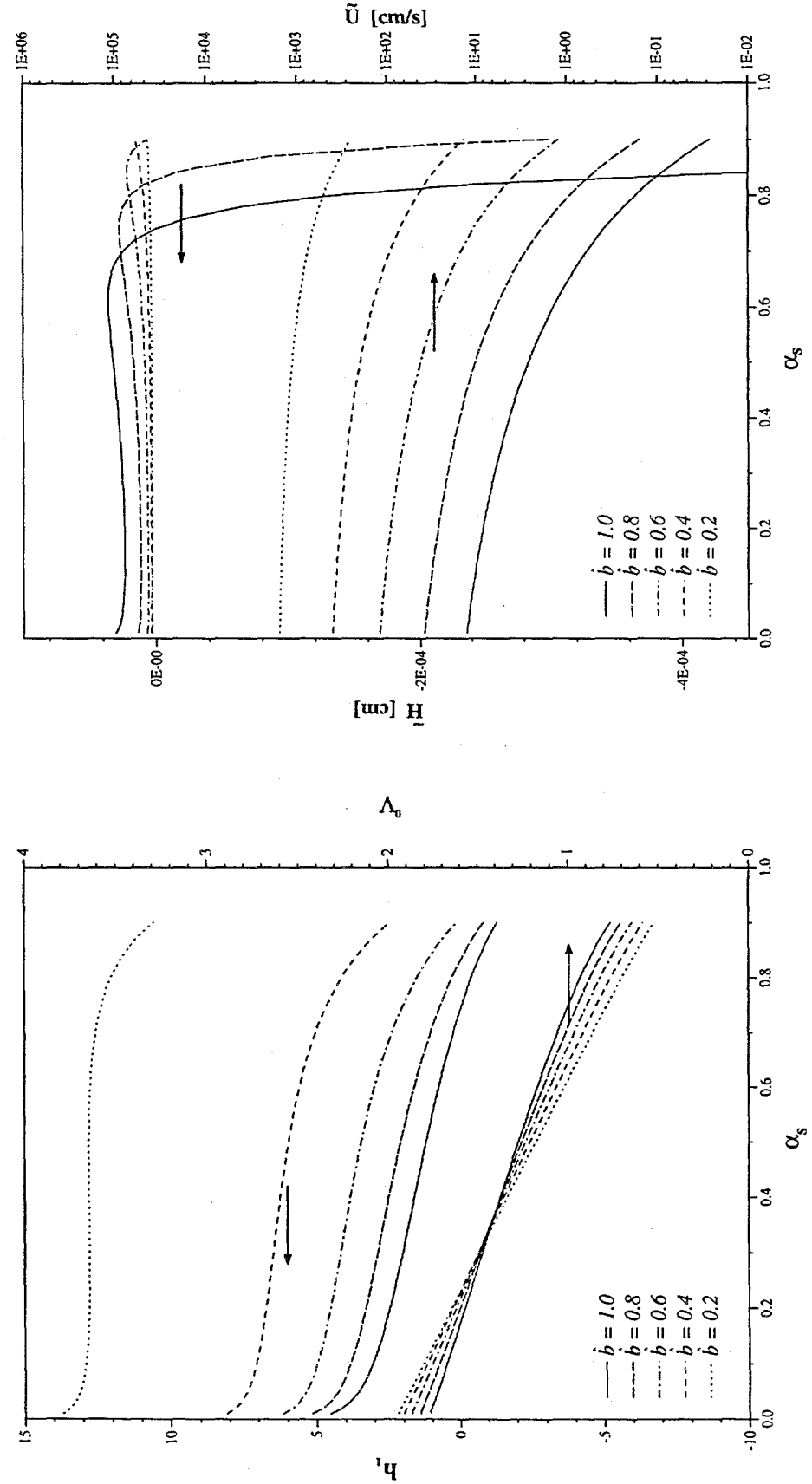
Ũ [cm/s]
1E+06
1E+05
1E+04
1E+03
1E+02
1E+01
1E+00
1E-01
1E-02
H̃ [cm]
0E-00
-2E-04
-4E-04
α_s
0.0
0.2
0.4
0.6
0.8
1.0
b̂ = 1.0
b̂ = 0.8
b̂ = 0.6
b̂ = 0.4
b̂ = 0.2
Λ_0
h_1
15
10
5
0
-5
-10
4
3
2
1
0

Figure 9a,b

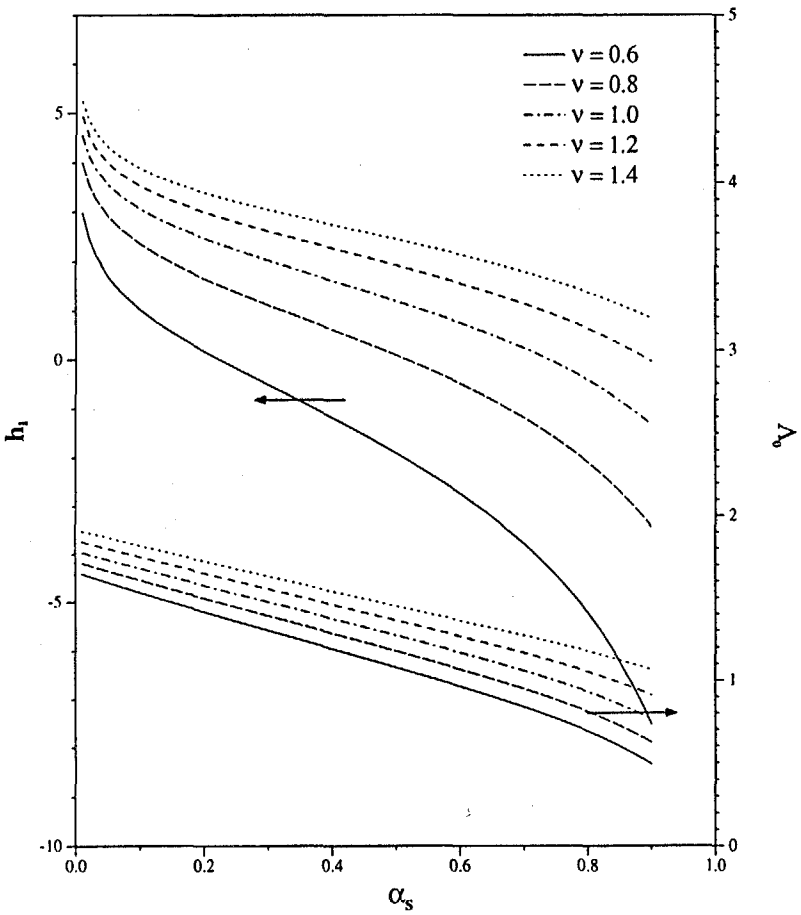

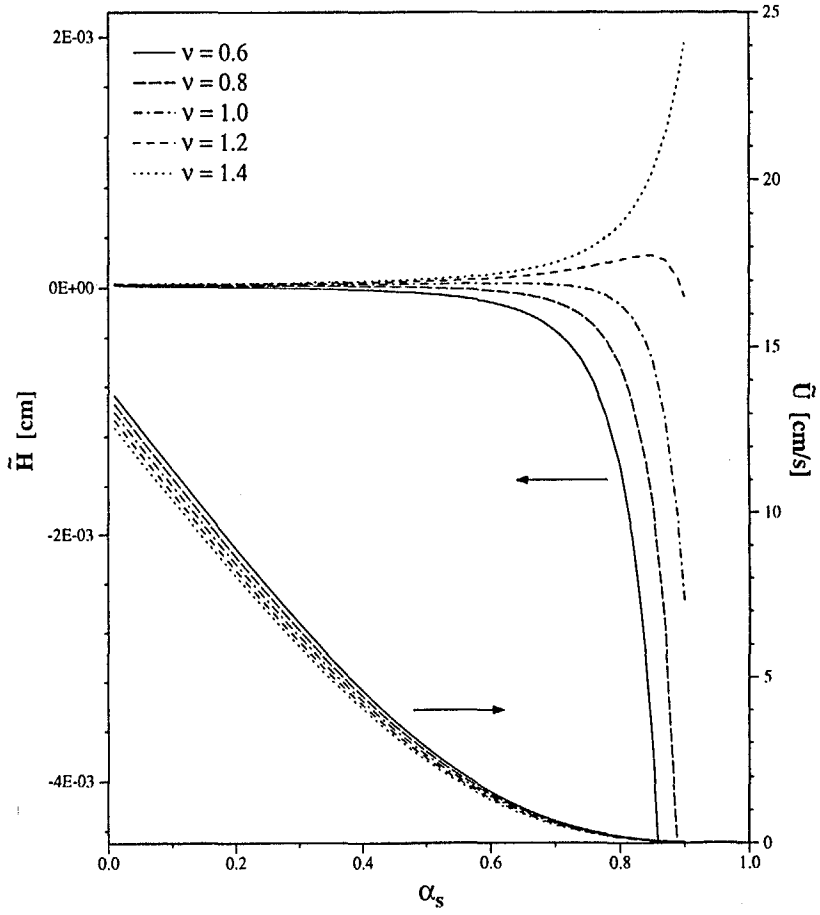

Figure 10a,b

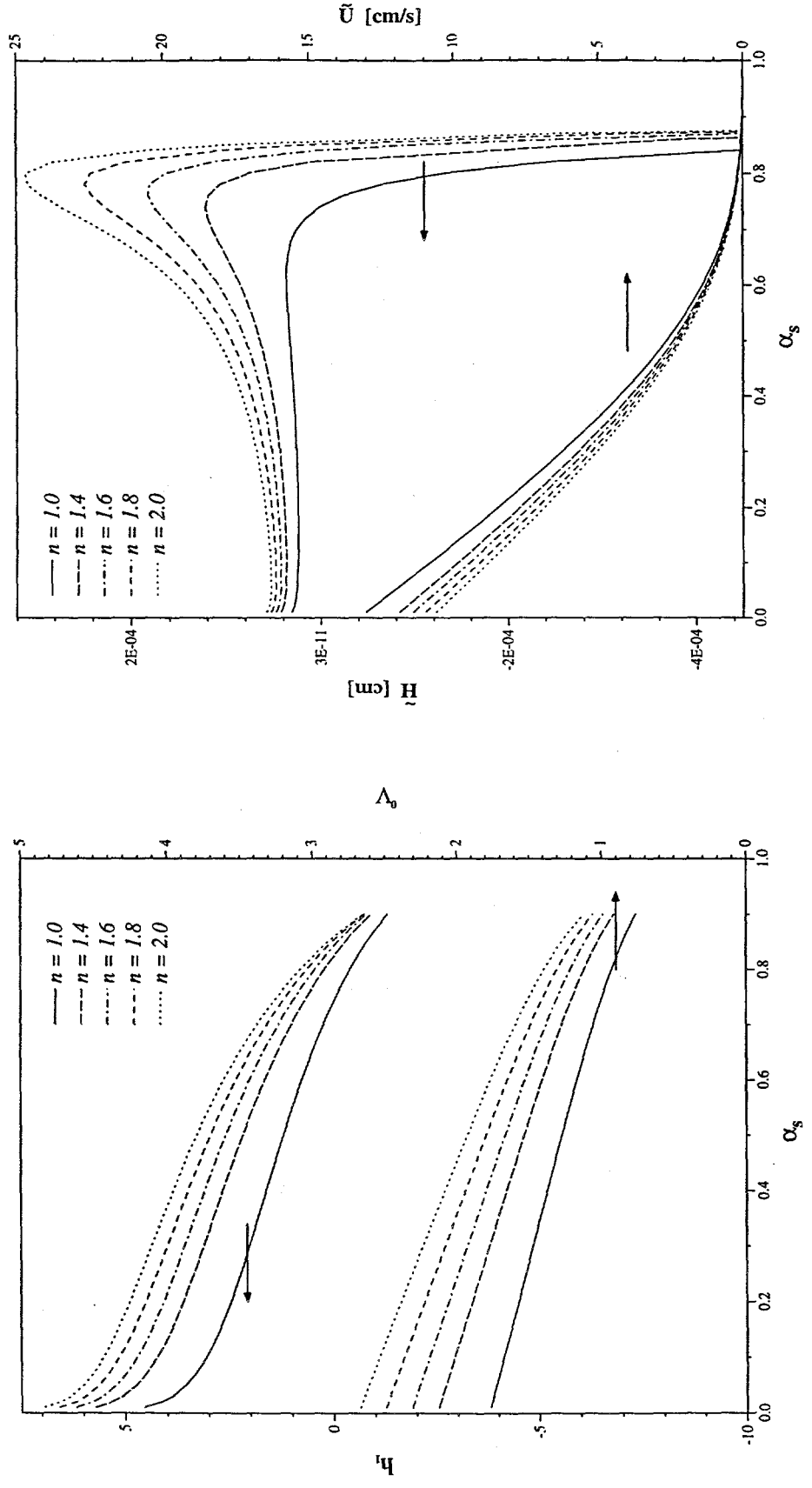
Ũ [cm/s]
25
20
15
10
5
0
1.0
0.8
0.6
0.4
0.2
0.0
α_s
n = 1.0
n = 1.4
n = 1.6
n = 1.8
n = 2.0
2E-04
3E-11
-2E-04
-4E-04
H̃ [cm]
Λ_0
5
4
3
2
1
0
h_1

Figure 11a,b

UNLIMITED RELEASE

INITIAL DISTRIBUTION

Dr. John K. Bechtold
Department of Mathematics
New Jersey Institute of Technology
Newark, NJ 07102-1982

Dr. Mitat A. Birkan
Program Manager
Directorate of Aerospace and Engineering Sciences
Department of the Air Force
Bolling Air Force Base, DC 20332-6448

Prof. Michael Booty
Department of Mathematics
New Jersey Institute of Technology
Newark, NJ 07102-1982

Prof. John D. Buckmaster
Department of Aeronautical and Astronautical Engineering
University of Illinois
Urbana, IL 61801

Prof. Sebastien Candel
Ecole Central des Arts et Manufactures
Grande Voie de Vignes
92290 Chatenay-Malabry
FRANCE

Dr. John Card
Department of Mechanical Engineering
Yale University
New Haven, CT 06520

Prof. J. F. Clarke
College of Aeronautics
Cranfield Institute of Technology
Cranfield-Bedford MK43 OAL
ENGLAND

Prof. Paul Clavin
Laboratoire Dynamique et Thermophysique des Fluides
Universite de Provence
Centre Saint Jerome
13397 Marseille Cedex 4
FRANCE

Prof. F. E. C. Culick
Jet Propulsion Center
California Institute of Technology
Pasadena, CA 91125

Prof. Martin Golubitsky
Department of Mathematics
University of Houston
University Park
Houston, TX 77004

Prof. Michael Gorman
Department of Physics
University of Houston
Houston, TX 77004

Dr. Daryl D. Holm
CNLS, MS 457
Los Alamos National Laboratory
Los Alamos, NM 87545

Prof. G. M. Homsy
Department of Chemical Engineering
Stanford University
Stanford, CA 94305

Dr. Guy Joulin
Laboratoirie D'Energetique et de Detonique
Universite de Poitiers
Rue Guillaume VII
86034 Poitiers
FRANCE

Dr. Hans Kaper
Applied Mathematics Division
Argonne National Laboratory
9700 S. Cass Ave.
Argonne, IL 60439

Prof. A. K. Kapila
Department of Mathematical Sciences
Rensselaer Polytechnic Institute
Troy, NY 12128

Prof. D. R. Kassoy
Department of Mechanical Engineering
University of Colorado
Boulder, CO 80309

Prof. Joseph B. Keller
Department of Mathematics
Stanford University
Stanford, CA 94305

Prof. Barbara Keyfitz
Department of Mathematics
University of Houston
University Park
Houston, TX 77004

Prof. C. K. Law
Department of Mechanical and Aerospace Engineering
Engineering Quadrangle
Princeton University
Princeton, NJ 08544

Dr. Gary Leaf
Applied Mathematics Division
Argonne National Laboratory
9700 S. Cass Avenue
Argonne, IL 60439

Prof. Amable Liñán
Universidad Politecnica de Madrid
Escuela Tecnica Superior de Ingenieros Aeronauticos
Plaza del Cardenal Cisneros, 3
Madrid - 3
SPAIN

Prof. J. T. C. Liu
Division of Engineering, Box D
Brown University
Providence, RI 02912

Prof. Moshe Matalon
Department of Engineering Sciences and Applied Mathematics
Northwestern University
Evanston, IL 60208

Prof. Bernard J. Matkowsky
Department of Engineering Sciences and Applied Mathematics
Northwestern University
Evanston, IL 60208

Prof. A. C. McIntosh
Department of Fuel and Energy
University of Leeds
Leeds LS2 9JT
UNITED KINGDOM

Prof. D. O. Olagunju
Department of Mathematical Sciences
University of Delaware
Newark, DE 19716

Prof. R. E. O'Malley
Department of Applied Mathematics
University of Washington Seattle, WA 98195

Prof. Norbert Peters
Institute fur Allgemeine Mechanik
Technische Hochschule Aachen
Aachen
GERMANY

Prof. John Ross
Department of Chemistry
Stanford University
Stanford, CA 94305

Prof. Victor Roytburd
Department of Mathematical Sciences
Rensselaer Polytechnic Institute
Troy, NY 12128

Prof. W. A. Sirignano
Office of the Dean
School of Engineering
University of California, Irvine
Irvine, CA 92717

Prof. L. Sirovich
Division of Applied Mathematics, Box F
Brown University
Providence, RI 02912

Prof. G. I. Sivashinsky
Department of Mathematics
Tel-Aviv University
Ramat-Aviv, Tel-Aviv 69978
ISRAEL

Prof. Mitchell D. Smooke
Department of Mechanical Engineering
Yale University
New Haven, CT 06520

Prof. D. Scott Stewart
Department of Theoretical and Applied Mechanics
University of Illinois
Urbana, IL 61801

Prof. C. H. Su
Division of Applied Mathematics, Box F
Brown University
Providence, RI 02912

Prof. Cesar Treviño
Departmento de Termica y Fluidos
Universidad Nacional Autonoma de Mexico
Facultad de Ingenieria
Patios No. 12, Jardines del Sur
MEXICO 23, D.F.

Prof. Vladimir Volpert
Department of Engineering Sciences and Applied Mathematics
Northwestern University
Evanston, IL 60208

Dr. David Weaver
Air Force Rocket Propulsion Laboratory
DYP/Stop 24
Edwards Air Force Base, CA 93523

Prof. Forman A. Williams
Department of Applied Mechanics and Engineering Sciences
University of California, San Diego
La Jolla, CA 92093

Prof. Vigor Yang
Department of Mechanical Engineering
Pennsylvania State University
University Park, PA 16802

Prof. Ben Zinn
Department of Aerospace Engineering
Georgia Institute of Technology
225 North Avenue, NW
Atlanta, GA 30332

C. K. Westbrook, LLNL, L-321

MS 1110 R. C. Allen, 1422
MS 0834 A. C. Ratzel, 9112
MS 0834 M. R. Baer, 9112
MS 0834 M. L. Hobbs, 9112
MS 0834 R. J. Gross, 9112

MS 9001 T. O. Hunter, 8000
MS 9405 R. E. Stoltz, 8008
MS 9004 M. E. John, 8100
MS 9213 S. C. Johnston, 8103
MS 9054 W. J. McLean, 8300
MS 9163 W. Bauer, 8302
MS 9042. C. M. Hartwig, 8345
MS 9056 L. A. Rahn, 8351
MS 9051 W. T. Ashurst, 8351
MS 9051 A. R. Kerstein, 8351
MS 9052 D. R. Hardesty, 8361
MS 9055 R. Behrens, 8361
MS 9052 S. B. Margolis, 8361 (30)
MS 9053 R. W. Carling, 8362
MS 9021 Technical Communications Department, 8815, for OSTI (10)
MS 9021 Technical Communications Department, 8815/Technical Library, MS 0899, 4414
MS 0899 Technical Library, 4414 (4)
MS 9018 Central Technical Files, 8950-2 (3)